CORNELL AERONAUTICAL LABORATORY, INC.
Flight Research Department

A STUDY OF TWO PROPOSED STABILIZATION TECHNIQUES FOR THE X-15 HORIZONTAL SURFACE CONTROL SYSTEM

CAL Report No. TB-1568-F-1

Contract No. NAS4-123

By: William R. Deazley
William R. Deazley

Approved: J. Norman Ball
J. Norman Ball,
Assistant Head,
Flight Research Department

Date: August 10, 1961

No. of Pages 84

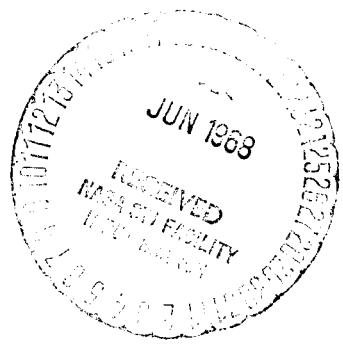

ABSTRACT

An analysis is presented of two proposed methods for providing additional gain margin in the stability augmentation loop of the X-15 horizontal surface control system. Expansion of the flight envelope to higher dynamic pressures, Mach numbers and altitudes has made it imperative to introduce refinements in the basic control system. The two methods considered in this report are the "notch filter" and "hydraulic pressure feedback" techniques. Both methods have considerable merit, but the pressure feedback approach appears to offer the most improvement.

FOREWORD

This study was performed at the Cornell Aeronautical Laboratory, Inc. under Contract NAS4-123, administered by the Control and Guidance Branch of the NASA Flight Research Center, Edwards, California. The study was primarily concerned with proposed stabilization techniques to be applied to the X-15 flight control system. Auxiliary data concerning structural interaction and aerodynamic damping were also to be obtained as part of the study. The assistance of Mr. Norman Cooper and Mr. Gene Farr of North American Aviation in obtaining the necessary background information and structural data is acknowledged, as is the aid and guidance of Mr. Larry Taylor, the NASA Project Engineer for this study.

TABLE OF CONTENTS

LIST OF ILLUSTRATIONS

TABLES

LIST OF SYMBOLS

A	Area of one piston face
A_T	Total area of piston faces
B	Bulk modulus of fluid, lb/ft^2
D	Denotes denominator or relating to denominator
$\|A\|\|B\|\|C\|\|D\|$	Determinants defined in text
$G(s)$	Transfer function (general form)
I_x	Moment of inertia of fuselage about its x axis
I_{xy}	Product of inertia (rigid body) for one horizontal stabilizer surface around its spindle axis and the fuselage center line
k	Load compliance (referenced to actuator) ft/lb
K	S.A.S. rate gyro feedback gain, $\frac{\text{degrees } \delta_A}{\text{deg/sec rolling rate}}$
K_1	Valve gain, $\frac{\text{flow rate}}{\text{unit valve displacement}}$ $\frac{ft^3/sec}{ft}$
K_2	Leakage between chambers, $\frac{ft^3/sec}{ft}$
K_3	Pressure feedback valve displacement gain, $\frac{ft}{lb/ft^2}$ or ft^3/lb
K_{sp}	Support compliance, ft/lb
K_s	Effective inertia at resonance
L_{δ_A}	Aerodynamic rolling moment due to horizontal stabilizer angle
m	Load inertia (referenced to actuator), slugs
m_c	Cylinder mass, slugs
m_p	Piston + support effective mass, slugs
N	Denotes numerator or relating to numerator
q	Dynamic pressure
Q	Quadratic factor

Q_c Volumetric rate resulting from cylinder motion, ft^3/sec

Q_e Volumetric rate error (determining internal pressure P), ft^3/sec

Q_p Volumetric rate resulting from piston motion, ft^3/sec

Q_x Fluid flow rate into cylinder, ft^3/sec

P Chamber pressure resulting from Q_e

V Volume of one chamber, ft^3

X_c Cylinder displacement, ft

X_i Input commanded cylinder displacement, ft

X_m Load displacement (referenced to actuator) ft

X_v Total valve displacement, ft

$X_{\Delta p}$ Valve displacement resulting from pressure feedback, ft

α Actuator friction (internal + linkages) $\frac{lb}{ft/sec}$

α_p Support friction, $\frac{lb}{ft/sec}$

β Load (horizontal surface) damping, $\frac{lb}{ft/sec}$

δ_A Horizontal stabilizer asymmetric input angle

Δ_D, Δ_N Remainder terms at resonance

Δ_1, Δ_2 Small numbers expressing frequency deviations

ζ Damping ratio

τ Time constant of first order approximation for actuator transfer function

τ_3 Pressure feedback time constant

ϕ Fuselage roll angle

ϕ_1, ϕ_2 Constants in $\Phi(s)$ transfer function

$\Phi(s)$ Fuselage roll to horizontal stabilizer angle transfer function

ω Radian frequency

ω_1 First mode frequency uncoupled

ω_2 Second mode frequency uncoupled

INTRODUCTION

Structural resonance effects have been observed in the horizontal stabilizer of the X-15 research aircraft. This resonance interferes with the proper operation of the control system. The horizontal surface, because of its construction, is a very low damped element. This poor damping plus the axial dissymmetry from the sweepback result in strong coupling of the surface resonance modes and the fuselage. This coupling is observed to be most effective in destabilizing the stability augmentation system (SAS) in the roll mode.

Two methods which have been proposed for preventing this poorly damped surface from limiting the effective gain of the SAS loop are analyzed in this report. The first of these methods discussed employs a "notch filter" in the SAS loop to selectively attenuate the first mode structural frequency. The other method discussed is the application of pressure feedback to the actuator valve to produce a more stable actuator plus load combination.

Background information about the form of the structural interaction and aerodynamic damping to be expected is also included in Appendixes.

DISCUSSION OF THE NOTCH FILTER TECHNIQUE

The "Notch Filter" method is especially attractive since the addition of such elements does not require major modifications in the surface power actuator. The Notch Filter capabilities are limited, however, since it is a fixed frequency device. Also, it would not actually improve the damping of the surface. Gust disturbances or other external influences would still be able to excite resonant bursts in t e surface. The fixed frequency characteristics of the notch are not too troublesome if the notch design provides a wide enough attenuation band to cover possible variations in the structural resonant frequency.

Appendix A is a detailed discussion and analysis of the results of introducing a notch filter into the SAS loop. Appendix B is a discussion of the transfer function of the structural interaction for the first two modes and Appendix F provides background information helpful in synthesizing the notch transfer function. The increase in allowable gain at the first mode results in a gain ratio (or gain margin) of the Notch Network versus no notch of $\frac{1.99}{0.0749} = 26.6$. The phase characteristic of the notch has been chosen so that phase shifts in the frequency range of the residual oscillation are negligible. Also the single mode picture of the phase characteristics in this region and the two mode picture are not significantly different.

The linear analysis indicated a very stable second mode resulting from introduction of the notch because of the phase contribution of the notch network at the second mode frequency. This stability characteristic has not been observed in the actual system. It is felt by the writer that some further increase in gain can be obtained by experimentally trying networks having phase shifts in the 214 rad/sec region and negligible phase shifts in the residual oscillation region. Since this portion of the analysis is not valid, any gain margin which would be calculated from the linear picture is subject to drastic changes when the system non-linearities are included. The notch filter does have some additional attenuation in the 214 rad/sec region which can be used as a possible indication of the allowable gain improvement between the case of no-notch and

the use of a notch network. If the non-linearities remain equally effective, then a gain increase of approximately 4:1 over the uncorrected allowable gain for the second mode is possible with the addition of the notch. This would result in an over-all gain margin of 4 x 0.78 / 0.074, or 40. This points to the fact that insufficient knowledge exists in the 214 rad/sec region to make anything but an "educated guess" about the gain margin.

One thing is certain: the first mode is effectively removed from the problem when a notch filter is introduced in the SAS loop. Possibly a second notch in the 214 rad/sec region would stabilize that mode also.

DISCUSSION OF THE PRESSURE FEEDBACK TECHNIQUE

While the "notch filter" technique can be considered to be a reasonable "first fix", it would still be better to correct the actual trouble resulting from the undamped surface-actuator combination. One approach which is most obvious is to use a horizontal stabilizer with more inherent damping. The next approach would be to provide artificial damping. With a relatively rigid actuator, external artificial damping is ineffective since the surface may be visualized as a cantilever with a relatively rigid supporting structure. Since the motion of the supporting structure (i.e., the actuator, etc.) is very small, very little damping can be coupled into the surface near its root.

If this artificial damping is applied through the actuator, however, it is possible to introduce actuator forces which are of the proper phase and amplitude to absorb the energy stored in the surface.

The most obvious approach to obtaining this artificial damping is by the use of pressure feedback to the actuator valve. This can be obtained by many techniques. Reference 1 describes an electrohydraulic valve which employs the pressure feedback technique to greatly improve servo performance. It is of course sketchy, analytically, since such information may be considered proprietary. Reference 2 considers many techniques which are similar to the the pressure feedback discussed later, but again, is also rather sketchy. References 3, 4, and 5 consider techniques employing pressure feedback on the essential equations of hydraulic actuators operating on high inertia loads. Reference 6 describes techniques for summing load reaction information into the control valve to stabilize large inertia loads. Very little work has been encountered which would apply to the specific problem discussed in Appendix C.

The results of Appendix C can be summarized as follows. Pressure feedback techniques can be applied to stabilize an actuator + resonant load configuration to a very marked degree. A systematic design technique and analysis is presented which results in practical values for the necessary

parameters to stabilize the servo system. No attempt was made in Appendix C to present a workable valve for the actuator configuration in the X-15.

Appendix D analyzes the SAS control loop, using an actuator of the type discussed in Appendix C. The maximum allowable gain K , $^{deg}/_{deg/sec}$ is found to be 2.54 as compared to 0.059 obtainable without any compensation. The gain margin, or gain improvement, that these results would indicate is 2.54 / 0.059 = 43. The actuator frequency response and phase shift are greatly improved with pressure feedback of the type analyzed. But the most important or significant improvement which is possible with pressure feedback is the allowable reduction in backlash, hysteresis and control cable compliance which is feasible without exciting the resonant surface.

The present actuator employed to deflect the horizontal stabilizer and the reflected load of the horizontal stabilizer are unstable at valve gains considerably below the present operating valve gain. The actual system remains stable only because of the control cable flexibility, hysteresis and deadband which effectively reduce the system gain. If these non-linearities are reduced, for example, by locking the SAS servo and the pilot input point, the surface actuator and its load exhibit the predicted instability.

Along with the structural resonance problem a non-linear oscillation, resulting from this hysteresis and deadband mentioned, must be kept below safe and tolerable limits. Any attempt to reduce the oscillations resulting from these non-linearities by reducing the size of these non-linearities only tends to destabilize the structural modes. This "residual" oscillation amplitude is a function of effective $L_{\delta_A} \times K$. The present system has marginal stability at large values of KL_{δ_A} . Pressure feedback stabilization allows these non-linearities to be reduced in size as much as is practically possible without destabilizing the structural modes thus affecting a reduction in the amplitude of the residual oscillation which would not be possible by any external fix such as the Notch Filter technique.

Actually the pressure feedback technique automatically generates a notch at the resonant modes of the actuator-load system. These "notches"

are inherent in the system equations since it is necessary, no matter what stabilization technique is used, to prevent actuator motions from existing at the resonant frequencies.

The question now arises – after this description of the capabilities of Pressure Feedback – is it possible to construct a reliable device (preferably all mechanical) which will operate the way the analysis has suggested. It appears that the answer to this question is yes. Not only is it possible to construct such a device, it is also very likely possible to construct one which will fit the present actuators without any major modifications in linkages, etc.

Appendix E describes such a valve schematically. Some comments should be included concerning some practical problems associated with constructing a pressure feedback valve. The linear picture employed in the analysis of Appendix C must be modified. The major non-linearity encountered is in the hydraulic high-pass network. The capillary used in determining the corner radian frequency, $1/\tau_3$, is too sensitive to temperature to be practical. A sharp edged orifice is used because it is relatively independent of viscosity. The flow-pressure characteristic of this type orifice is parabolic, thus the time constant τ_3 is amplitude dependent. For small amplitudes, the τ_3 value is very small. This will tend to produce a small amplitude limit cycle oscillation whenever the actuator has no input commands.

CONCLUSIONS

Structural interaction and damping has been calculated for the horizontal surface and fuselage. This data, together with pertinent flight control system data, has been used to determine the effects of two proposed stabilization techniques for the horizontal surface control system. It has been shown on the basis of a linear analysis that both techniques are able to provide a relatively high degree of system stabilization. The model of the actuator employed in the notch filter analysis is idealized to such an extent that the non-linearities would modify the available stabilization of the second structural mode (first torsion). The interaction between the actuator and its resonant load is controllable by pressure feedback techniques. The Stability Augmentation System employing pressure feedback - stabilized actuators appears to be the most effective way to improve the stability of the X-15 flight control system.

Analysis of a complex resonance phenomenon which is further confused by uncertain amounts of non-linearities must always depend upon careful consideration of the effects of these non-linearities on the linear picture. One must not require the corrective action to be applied in such a manner where the non-linearities are significant and could drastically reduce the effectiveness of the desired correction. Pressure feedback techniques are very effective when considered in the linear analysis, but care must be taken to not have non-linearities such as valve driction, hysteresis and deadband of such an amplitude that they are detrimental to the operation of the pressure feedback portion of the control system. In a similar fashion, the linear picture of the notch filter corrective technique is very promising. Non-linearities of the type which produce phase shifts in the system are vapable of destabilizing certain modes of oscillation which are otherwise quite stable. This is apparently occurring in the X-15 horizontal surface SAS loop since the linear analysis predicts a very stable system resulting from the use of the notch filter to stabilize the SAS loop. One can envision an iterative technique employing notch filters to reduce the gain at successive resonance modes until the over-all SAS loop gain can be increased to the desired limits. This would, of course, be a tedious and time-consuming task and it is quite possible that

aerodynamic effects and temperature changes would shift the resonant modes (especially the higher modes) enough to make such an approach ineffective.

It is felt by the writer that application of the pressure feedback technique is potentially a better approach and should also be investigated on an experimental basis. Although only one structural mode was included in the analysis, the trend observed in the analysis, i.e., the manner in which certain portions of the equations behaved, seemed to indicate that additional modes would also be stabilized with little or no difficulty.

REFERENCES

1. Geyer, L.H.: Controlled Damping Through Dynamic Pressure Feedback. Technical Bulletin #101. Moog Valve Co., Inc.

2. Blanton, J.W. and Grey, S.A.: Mechanical Feedback Improves Hydraulic Servovalves. Control Engineering, Vol. 6, No. 7, pp 111-113. July 1959.

3. Shearer, J.L. and Lee, S.T.: Selecting Power Control Valves - Their Design and Performance. Control Engineering, Vol. 3, No. 4, pp 73-76. April 1956.

4. Shearer, J.L.: Dynamic Characteristics of Valve Controlled Hydraulic Servomotors. Transactions of the ASME, Vol. 76, No. 6, pp 895-905.

5. Gold, H.; Otto, E.W.; and Ransom, V.L.: An Analysis of the Dynamics of Hydraulic Servomotors Under Inertia Loads and the Application to Design. Transactions of the ASME, Vol. 75, No. 10, pp 1383 - 1394.

6. Nightingale, J.M.: Aircraft Booster Design. Control Engineering, Vol. 2, No. 1, pp 49-56. January 1955.

7. Johnson, C.L.: Analog Computer Techniques. McGraw Hill Publishing Company. 1956.

APPENDIX A

ANALYSIS OF THE NOTCH FILTER TECHNIQUE FOR STABILIZATION OF STRUCTURAL MODE EFFECTS

The major reason for the employment of a notch filter for the reduction of structural resonance effects on a servo actuator is that it provides high attenuation of the frequency band in the vicinity of the particular structural mode.

The notch filter chosen for stabilizing the SAS loop for the 12 - 14 cycle resonance of the horizontal surface of the X-15 also had additional boundary conditions. The phase lag in the 0 - 4 cycle region must be very low so that the inclusion of a notch filter does not increase the residual oscillation amplitude.

With these requirements in mind a notch filter transfer function was obtained experimentally at NASA Flight Test Center which had these specifications and which did stabilize the structural mode in the 12-14 cycle region. It was observed on the X-15 however, that the torsion mode at 34 cps became unstable at a gain level only a moderate amount above the original gain.

The discussion that follows employs a linear picture of the SAS system and analyzes the SAS system with and without the notch filter for the effects of one and two structural modes.

The SAS loop equations will be considered in their order of increasing complexity.

CASE I - Normal SAS Loop with One Structural Mode

Using the root locations of the SAS servo, shaping, and gyro provided by NAA, the SAS loop block diagram (Figure 1) becomes:

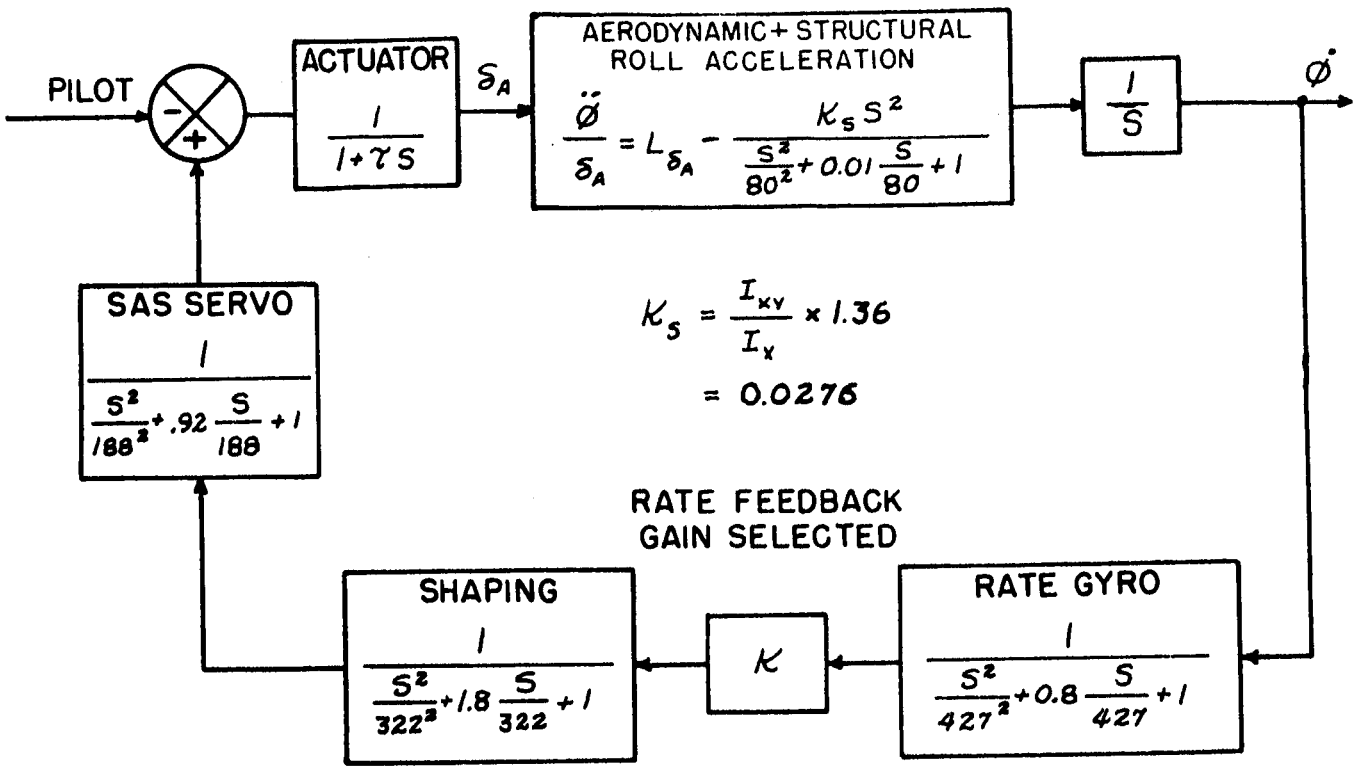

Figure A-1 SAS Loop Block Diagram

Since the problem of stabilizing the SAS loop exists at zero dynamic pressure and is relatively unchanged for small L_{δ_A} values, L_{δ_A} is assumed zero. The resulting roots of the characteristic equation for the SAS loop are:

one zero at: $S = 0$

poles at:

$S = -0.4 \pm j80$ ($\omega = 80$, $\zeta = 0.005$)

$S = -171 \pm j391.5$ ($\omega = 427$, $\zeta = 0.40$)

$S = -290 \pm j140$ ($\omega = 322$, $\zeta = 0.90$)

$S = -86.5 \pm j166.8$ ($\omega = 188$, $\zeta = 0.46$)

$S = -1/\tau = -6.667$ for $\tau = 0.15$ sec

The critical pair of roots is located at $-0.4 \pm j80$, therefore a detailed look at the root locus in the region around $-0.4 + j80$ is necessary. The departure angle of the root locus originating from $-0.4 + j80$ and the loop gain level in the immediate region about this root provide sufficient information to determine the

maximum system gain allowed for stability of the over-all loop, i.e., the gain at which some root crosses the imaginary axis into the right half plane.

A summary of the phase lags contributed to the phase at -0.4 +j80 is:

SAS	-26.0°
Gyro	-9.0°
Shaping	-25.8°
Actuator	-85.5°

The sum of these lags is -146.3°
Therefore, the departure angle from the pole at -0.4 +j80 is 180° - 146.3° = 33.7°.

The product of the distances of the poles to the -.4 +j80 point divided by the distance from the zero and the radial distances from the origin to the poles determine an approximate value for K for each unit distance from the pole at -0.4 +j80.

$$K = r \frac{121}{188} \times \frac{261}{188} \times \frac{499}{427} \times \frac{365}{427} \times \frac{363}{322} \times \frac{296}{322} \times \frac{80.3}{6.667} \times \frac{160}{80} \times \frac{1}{80} \times \frac{1}{80} \times \frac{I_x}{I_{xy}}$$

$$K = 0.00338\, r \left(\frac{I_{xy}}{I_x}\right)^{-1}$$

. For the calculated effective I_{xy}/I_x = 1.36 x 0.02027 = 0.0276 and r = 0.4 / cos 33.7° = 0.481 K = 0.059 $\frac{\text{deg}}{\text{deg/sec}}$ (this compares reasonably well with the NASA calculated 0.1 gain when the I_{xy}/I_x value of 0.015 is used).

To summarize Case I, the root at -0.4 +j80 and its conjugate are the two roots of the SAS loop which first cross the imaginary axis with increasing SAS loop gain. The gain K has been found to be about 0.059 for the calculated value of I_{xy}/I_x . The departure angle is +33.7° (positive counterclockwise).

If one considers the total loop gain through the structure I_{xy}/I_x K the root locus crosses at a gain of

$$K \frac{I_{xy}}{I_x}\Bigg|_{EFFECTIVE} = 0.00163$$

Fig. A-2 is an ESIAC root locus of the over-all SAS loop locus. The gain values indicated are for

$$K \frac{I_{xy}}{T}\Bigg|$$

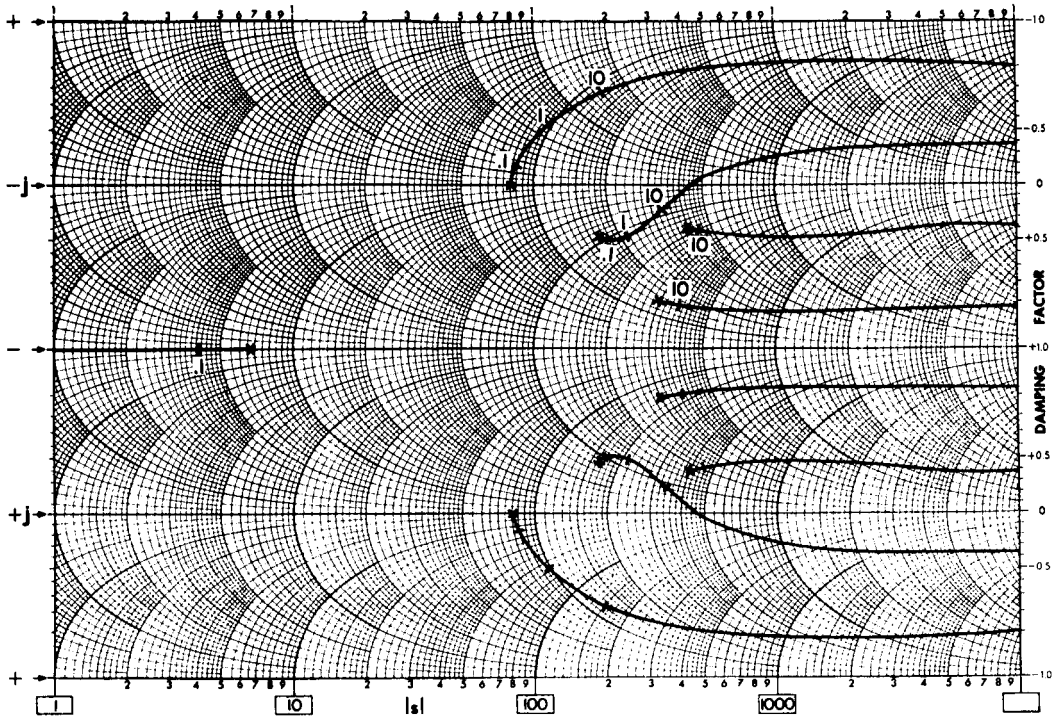

Figure A-2 SAS Loop, First Mode Only

CASE II - Normal SAS Loop With First Two Structural Modes

Appendix B discusses the structural transfer function in considerable detail. The transfer function which will be used in this discussion is

$$\bar{\phi}(s) = \frac{\frac{I_{xy}}{I_x}\left(\frac{s^2}{194^2} - 1\right)}{\left(\frac{s^2}{80^2} + .01\frac{s}{80} + 1\right)\left(\frac{s^2}{214^2} + .01\frac{s}{214} + 1\right)}$$

as $S \rightarrow 0$, $\ddot{\Phi}$ has a negative value. This is consistent with a right hand set of coordinates. At low frequencies, the structural interaction produces a counterclockwise roll of the fuselage for a clockwise spindle angle input. This is in the same direction as the roll produced by aerodynamic moments. Thus, independent of the way the coordinate system is defined, one must have a set of loop equations where the low frequency structural interaction for fuselage roll is of the same phase as the aerodynamically induced roll for a horizontal stabilizer deflection.

The "Aerodynamic and Structural Roll Acceleration" block in Figure A-1 will therefore have the following transfer function

$$\frac{\ddot{\phi}}{\delta_A} = -S^2 \left[\frac{1.36 \frac{I_{xy}}{I_x}}{\frac{S^2}{80^2} + .01 \frac{S}{80} + 1} - \frac{0.36 \frac{I_{xy}}{I_x}}{\frac{S^2}{214^2} + .01 \frac{S}{214} + 1} \right]$$

which is approximately

$$\frac{\ddot{\phi}}{\delta_A} = -S^2 \frac{I_{xy}}{I_x} \quad \frac{-\frac{S^2}{194^2} + 1}{\left(\frac{S^2}{80^2} + .01 \frac{S}{80} + 1\right)\left(\frac{S^2}{214^2} + .01 \frac{S}{214} + 1\right)}$$

Fig. A-3 is an ESIAC root locus plot of this case. The departure angle of the first mode is relatively unchanged. The locus of the second mode pole at 214 rad/sec has a departure angle of 71.6° counterclockwise (calculated).

It is worth noting here that the denominator has a form

$$1 - \frac{s(Q_{194}) \frac{I_{xy}}{I_x} K}{(Q_{80})(Q_{214})(Q_{427})(Q_{322})(Q_{188})(1 + \tau_3)} = D$$

where the Q_i are the quadratic factors for the gyro, SAS servo, etc. This function D is the form which is solved by a "zero degree" root locus.

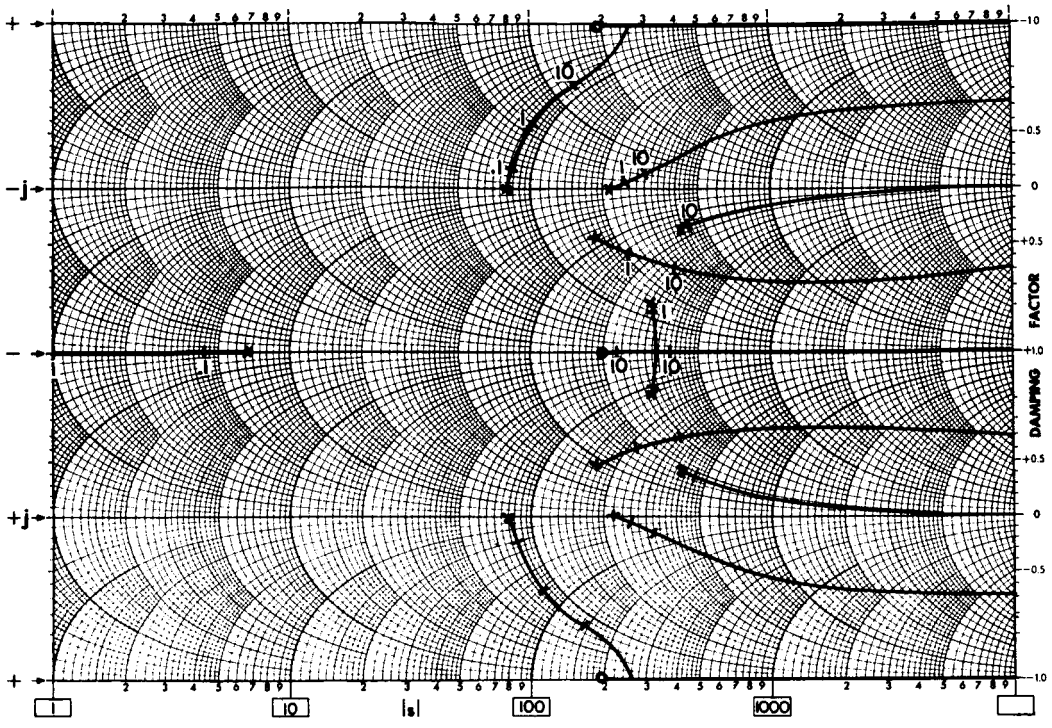

Figure A-3 SAS Loop, First Mode and Second Mode

The gain K required to drive the first mode roots unstable is modified slightly by inclusion of the zeros and second mode poles.

The gain is modified by a factor of 0.934. Thus

$$K = 0.934 \times 0.00338 \times 0.481 \left(\frac{I_{XY}}{I_X}\right)^{-1}$$

$$= 0.934 \times \underbrace{\frac{0.00338}{0.02027} \times 0.481}_{.0802}$$

$$K = 0.0749$$

therefore, the first mode is unstable for total loop gains of K^{I_{XY}/I_X} exceeding 0.00152.

The gain required to drive the second mode roots unstable can be

calculated by geometry to be

$$K = \frac{214}{6.667} \times \frac{247}{427} \times \frac{628}{427} \times \frac{300}{322} \times \frac{459}{322} \times \frac{98}{188} \times \frac{388}{188} \times \left(\frac{194}{290}\right)^2 \times \frac{134}{80} \times \frac{294}{80} \times \frac{428}{214} \times \frac{r}{214^2} \times \frac{I_x}{I_{xy}}$$

and $$r = \frac{0.005 \times 214}{\cos 71.6^\circ} = 3.39$$

therefore $$K = \frac{3.39 \times 0.00467}{0.02027} = 0.780$$

The maximum total loop gain which is used for the root locus plots, i.e., $K \frac{I_{xy}}{I_x}$ for instability is .01583

To summarize Case II, the major results from including the second mode are:

a. The maximum stable gain of the first mode is changed slightly from 0.059 to 0.075. The departure angle is unchanged.

b. The second mode departure angle was computed to be 71.6° counterclockwise and the maximum stable gain was calculated to be 0.78.

CASE III - SAS Loop Plus First and Second Structural Modes and NAA-NASA Notch Filter

Since the notch filter selected by NAA and NASA was primarily intended to attenuate the frequency band around the first structural mode, this frequency band will be explored first.

The notch filter transfer function selected is:

$$G(S) = \frac{\left(\frac{S^2}{41.8^2} + 2.4\frac{S}{41.8} + 1\right)\left(\frac{S^2}{80^2} + 0.125\frac{S}{80} + 1\right)}{\left(\frac{S^2}{41.8^2} + 0.24\frac{S}{41.8} + 1\right)\left(\frac{S^2}{80^2} + 7.5\frac{S}{80} + 1\right)}$$

The roots of $G(S)$ are located at:

Zeros:

$S = -78, -22.4$ ($\omega = 41.8$, $\zeta = 1.2$)

$S = -5.0 \pm j79.8$ ($\omega = 80$, $\zeta = 0.0625$)

Poles:

$S = -5.01 \pm j41.5$ ($\omega = 41.8$, $\zeta = 0.12$)

$S = -589, -10.87$ ($\omega = 80$, $\zeta = 3.75$)

In the region around -0.4 +j80, the only root which is relatively close is the zero at -5.0 +j79.8. If the gain and phase contributions of all the roots are calculated for this region, then it is possible to obtain an accurate approximation for the locus and the effective K values resulting from the notch filter.

The filter gain at j80 is: (using distances from the roots to the +j80 point)

$$\frac{589}{594.5} \times \frac{10.9}{80.75} \times \frac{41.8}{38.8} \times \frac{41.8}{121.6} \times \frac{111.4}{78} \times \frac{83}{22.4} \times \frac{5}{80} \times \frac{159.8}{80} = \frac{1}{30.5} = 0.0324$$

The phase contribution of the notch filter to the departure angle of the root at -0.4 +j80 is -51.3°.

Thus the departure angle of the locus from the pole at -0.4 +j80 is:

$$33.7 - 51.3 = -17.6 \text{ (i.e., } 17.6° \text{ clockwise)}$$

Since this departure angle is small, the locus will cross the $j\omega$ axis in a region close to the j80 point. Thus the gain contribution resulting from the distance between the crossing point of the locus and the $j\omega$ axis and the root at -5.0 +j79.8 is still nearly 1/5.

The distance from -0.4 +j80 to the locus intersection with the $j\omega$ axis is approximately

$$\frac{0.4}{\cos 17.6°} = 0.42$$

Thus the total loop gain required to make the SAS loop unstable at the first structural mode is:

$$K\frac{I_{xv}}{I_x} = 30.5 \times 0.00152 \times \frac{.420}{.481} = 0.0405$$

where the 30.5 is the gain improvement resulting from the notch filter attenuation and the ratio .420/.481 is the ratio of distances of the intersection of the two loci and the $j\omega$ axis from the pole at -0.4 +j80. The factor 0.00152 is the maximum total stable loop gain with no notch filter.

Thus, if $I_{xv}/I_x = 0.02027$, the gain K required to produce instability at the first structural mode is 1.99.

Figure 4 is an ESIAC root locus plot of the SAS loop including the two structural modes and notch filter. The roots located at -5 +j41.8 cross the $j\omega$ axis at a gain of approximately 0.6. Also, it should be noted that the second structural mode roots now have an advantageous departure angle and they cross the $j\omega$ axis at a total loop gain of about 10. Thus it would seem that the notch filter has "gain stabilized" the first mode and "phase stabilized" the second mode.

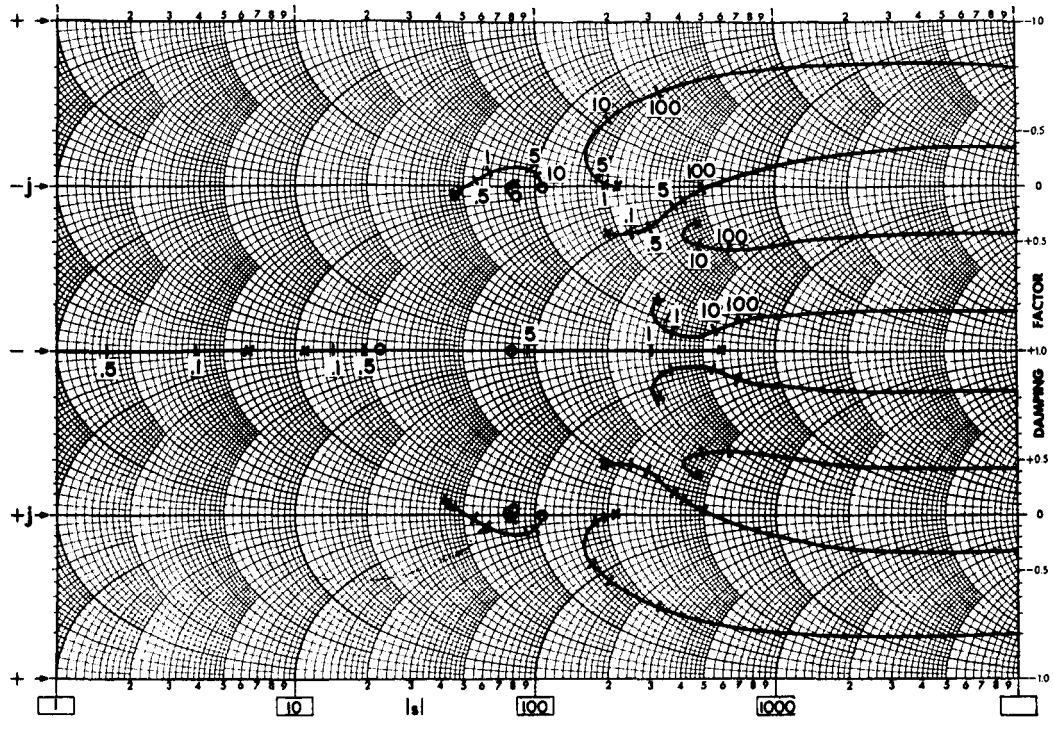

Figure A-4 SAS Loop, First Mode and Second Mode Plus Notch Filter

The departure angle of the second mode root locus, sans filter, is +71.6°; the additional phase contribution resulting from the notch filter at 214 rad/sec is +45°. The departure angle is therefore rotated this amount to a value of +116.6° (counterclockwise) which is in a direction of increased damping.

Unfortunately, the physical entity does not exhibit this extreme stability predicted above. The mechanism (non-linearities, additional coupling effects, etc.) which produces this instability is beyond the scope of this discussion. It would still be possible, though, to add phase stability to this situation by providing phase shift at this 214 rad/sec region sufficient to "phase stabilize" this mode similar to the above picture. Of course, large amplitude non-linearities again destabilize this mode - but possibly at a higher gain.

To summarize Case III, the notch filter provides considerable gain improvement insofar as stabilizing the first structural mode. The linear analysis

also resulted in a stable second mode which is not the case in reality. The root locus of the second structural mode remains close to the $j\omega$ axis, thus allowing any inherent non-linearities to easily de-stabilize it.

A simple phase locus plot can illustrate what can possibly be happening:

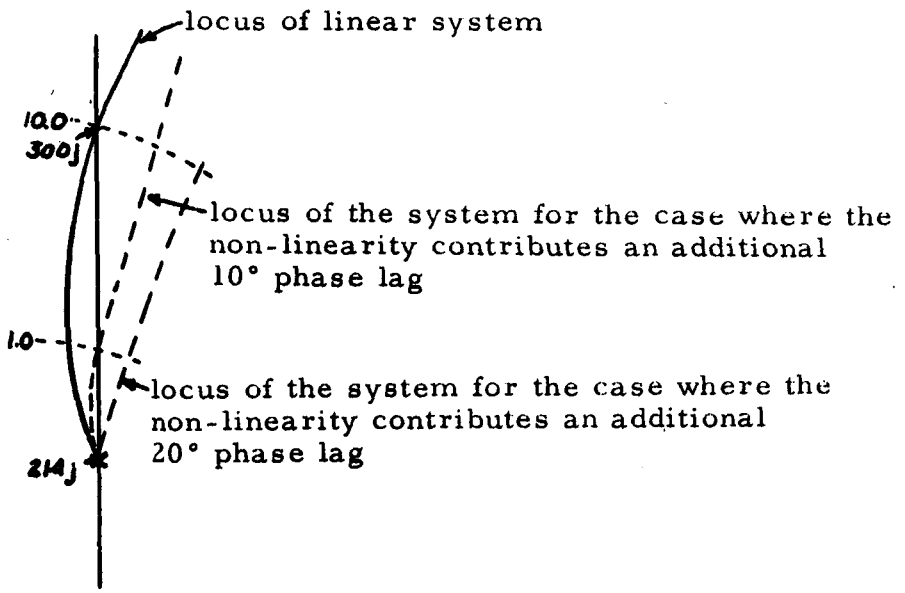

It is possible to improve the allowable loop gain by properly "phase stabilizing" the second mode. Whether phase lead or phase lag would be the most effective cannot be determined theoretically. "Cut and try" techniques must be used.

APPENDIX B

CALCULATION OF STRUCTURAL INTERACTION FOR FIRST BENDING AND FIRST TORSION MODES OF THE HORIZONTAL STABILIZER ON FUSELAGE ROLL

If only the first two normal modes of the stabilizer are considered (i.e., first bending and first torsion) the resultant transfer function for fuselage roll as a function of horizontal surface spindle angle including the effects of all shear and moments consists of a quartic over a quartic. This is recognized to be inaccurate as $S \rightarrow \infty$ but since this is only the second extension beyond the rigid body picture, it is not surprising that the transfer function has this form.

Actually, the calculated interaction terms are very nearly correct to cancel out the S^4 term. Therefore, the order of the numerator equation would be automatically only second.

The fuselage roll / stabilizer angle transfer function, $\Phi(s)$, can be expressed as

$$\Phi(s) \equiv \frac{\phi(s)}{\delta_A(s)} \tag{B-1}$$

$$= -\frac{I_{xy}}{I_x}\left[\frac{(s^2+\omega_1^2)(s^2+\omega_2^2) - \phi_1 s^2(s^2+\omega_2^2) - \phi_2 s^2(s^2+\omega_1^2)}{(s^2+\omega_1^2)(s^2+\omega_2^2) - \phi_3 s^2(s^2+\omega_2^2) - \phi_3 s^2(s^2+\omega_1^2)}\right] \tag{B-2}$$

(omitting the damping terms, which are small).

The calculated values of I_{xy}/I_x, ϕ_1, ϕ_2, etc. are

$$I_{xy} = 2347 \text{ lb ft}^2$$

$$I_x = 3600 \times 32.2 \text{ lb ft}^2$$

$$I_{xy}/I_x = 0.02027$$

$$\phi_1 = 1.35$$

$$\phi_2 = -0.3698$$

$$\phi_3 = \frac{10.65 \times 10^3}{I_x} = 0.092$$

$$\phi_4 = \frac{1.417 \times 10^3}{I_x} = 0.0122$$

The resultant equation for $\Phi(s)$ (omitting damping) has a numerator function

$$+0.0198\, s^4 - 7260\, s^2 + 2.93 \times 10^8 = 0$$

The accuracy of the calculations for ϕ_1 and ϕ_2 are not on such a rigid foundation with respect to the structural data that a slight readjustment cannot be allowed to simplify the form. The resultant resonant peak heights are not materially affected by the change.

If one sets $\phi_1 = 1.36$ and $\phi_2 = -0.36$, the numerator of $\Phi(s)$ reduces to

$$s^2 \left[\omega_1^2 (1-\phi_2) + \omega_2^2 (1-\phi_1) \right] + \omega_1^2 \omega_2^2 = 0$$

$$s^2 \left[\omega_1^2 \times 1.36 - \omega_2^2 \times 0.36 \right] + \omega_1^2 \omega_2^2 = 0$$

$$7780\, s^2 - 2.93 \times 10^8 = 0$$

yielding roots at

$$s = \pm 194 \text{ rad/sec}$$

For small damping, the roots of the denominator,

$$\left[1 - (\phi_3 + \phi_4)\right] s^4 + \left[\omega_1^2 (1-\phi_4) + \omega_2^2 (1-\phi_3) \right] s^2 + \omega_1^2 \omega_2^2 = 0$$

are $s = \pm j84.2$ and $s = \pm j215$

Small values of damping do not affect the imaginary parts of the roots.

These approximations are not accurate, of course, when computing the height of the resonant peaks. The damping must also be included.

Expanding the denominator of (B-2) with damping terms included results in:

$$(1-\phi_3-\phi_4)s^4+\left[2\zeta_1\omega_1(1-\phi_4)+2\zeta_2\omega_2(1-\phi_3)\right]s^3$$
$$+\left[\omega_1^2(1-\phi_4)+\omega_2^2(1-\phi_3)+4\zeta_1\zeta_2\omega_1\omega_2\right]s^2$$
$$+(2\zeta_1\omega_1\omega_2^2+2\zeta_2\omega_2\omega_1^2)s+\omega_1^2\omega_2^2 = D \qquad \text{(B-3)}$$

For small ζ_1 and ζ_2, resonance exists when

$$(1-\phi_3-\phi_4)s^4+(\omega_1^2+\omega_2^2-\phi_3\omega_2^2-\phi_4\omega_1^2)s^2+\omega_1^2\omega_2^2 = 0 \qquad \text{(B-4)}$$

At resonance the remainder in the denominator becomes

$$\left[2\zeta_1\omega_1(1-\phi_4)+2\zeta_2\omega_2(1-\phi_3)\right]s^3+4\zeta_1\zeta_2\omega_1\omega_2 s^2$$
$$+(2\zeta_1\omega_1\omega_2^2+2\zeta_2\omega_2\omega_1^2)s = \Delta_D \qquad \text{(B-5)}$$

Resonance occurs at s values close to $j\omega_1$ and $j\omega_2$. The remainder, Δ_D is not too sensitive to values of ω, therefore $j\omega_1(1+\Delta_1)$ and $j\omega_2(1+\Delta_2)$ are reasonably accurate values for substitution into Δ_D, where $\omega_1(1+\Delta_1)$ and $\omega_2(1+\Delta_2)$ are obtained from solving for the roots of (B-4), Δ_1 and Δ_2 are small quantities.

Since the odd power terms are the only significant ones in (B-5), setting $s = j\omega$ results in

$$\frac{\Delta_D}{j} = 2\zeta_1\omega_1\omega_2\left[\omega_2^2 - \omega^2(1-\phi_4)\right] + 2\zeta_2\omega_2\omega\left[\omega_1^2 - \omega^2(1-\phi_3)\right] \qquad \text{(B-6)}$$

if $\omega = \omega_1(1+\Delta_1)$ and $\zeta_2 = \zeta_1 = \zeta$

$$\frac{\Delta_{D_1}}{2j\zeta} = \omega_1^4(1+\Delta_1)^3\left[\frac{\omega_2^2}{\omega_1^2(1+\Delta_1)^2} - 1 + \phi_4\right]$$

$$+ \omega_2 \times \omega_1^3(1+\Delta_1)^3\left[\frac{\omega_1}{\omega_1^2(1+\Delta_1)^2} - 1 + \phi_3\right]$$

For small Δ_1 , this reduces to

$$\frac{\Delta_{D_1}}{2j\zeta} = \omega_1^3\omega_2(1+3\Delta_1)\left[\frac{\omega_2}{\omega_1}(1-2\Delta_1) - \frac{\omega_1}{\omega_2} + \frac{\omega_1}{\omega_2}\phi_4 + \phi_3 - 2\Delta_1\right] \qquad \text{(B-7)}$$

since $\Delta_1 = \frac{\omega_{RESONANCE}}{\omega_1} - 1$ for this case
$\omega_{RESONANCE}$ = 84 rad/sec if ω_1 = 80 radians,
therefore Δ_1 = 0.05.

$$\frac{\Delta_{D_1}}{2j\zeta} = \omega_1^3\omega_2 \times 1.15\left[2.675(0.9) - .374 + .374 \times 0.0122 + 0.092 - 0.10\right]$$

$$= 2.335\,\omega_1^3\omega_2$$

where ϕ_1 = 1.36, ϕ_2 = -0.36, ϕ_3 = 0.092, ϕ_4 = -.0122

ω_1 = 80 rad/sec, and ω_2 = 214 rad/sec.

In a similar fashion, the value for the denominator at the second resonant mode can be computed to be

$$\frac{\Delta_{D_2}}{2j\zeta} = (1+3\Delta_2)\omega_1\omega_2^3\left[\frac{\omega_1}{\omega_2}(1-2\Delta_2) - \frac{\omega_2}{\omega_1} + \frac{\omega_2}{\omega_1}\phi_3 + \phi_4 - 2\Delta_2\right] \quad \text{(B-8)}$$

$\omega_{RESONANCE}$ = 215 rad/sec, ω_2 = 214 rad/sec, Δ_2 = 0.00467

$$\therefore \frac{\Delta_{D_2}}{2j\zeta} = 1.014\,\omega_1\omega_2^3\left[0.374(.991) - 2.675 + 0.246 + 0.0122 - 0.00934\right]$$

$$\frac{\Delta_{D_2}}{2j\zeta} = 2.035\,\omega_1\omega_2^3$$

The numerator of Equation B-2 when expanded has the form

$$\begin{aligned}&(1-\phi_1-\phi_2)s^4 + \left[2\zeta_1\omega_1(1-\phi_2) + 2\zeta_2\omega_2(1-\phi_1)\right]s^3 \\ &+ \left[\omega_1^2(1-\phi_2) + \omega_2(1-\phi_1) + 4\zeta_1\zeta_2\omega_1\omega_2\right]s^2 \\ &+ (2\zeta_1\omega_1\omega_2^2 + 2\zeta_2\omega_2\omega_1^2)s + \omega_1^2\omega_2^2 = N\end{aligned} \quad \text{(B-9)}$$

Substituting the condition for resonance (Equation B-4) results in a remainder in the numerator

$$\begin{aligned}\Delta_N = &(-\phi_1 - \phi_2 + \phi_3 + \phi_4)s^4 + \left[2\zeta_1\omega_1(1-\phi_2) + 2\zeta_2\omega_2(1-\phi_1)\right]s^2 \\ &+ \left[4\zeta_1\zeta_2\omega_1\omega_2 - (\phi_1-\phi_3)\omega_2^2 - (\phi_2-\phi_4)\omega_1^2\right]s^2 + (2\zeta_1\omega_1\omega_2^2 + 2\zeta_2\omega_2\omega_1^2)s\end{aligned} \quad \text{(B-10)}$$

For small ζ_1 and ζ_2

$$\Delta_N = \left[(\phi_3-\phi_1) + (\phi_4-\phi_2)\right]s^4 + \left[(\phi_3-\phi_1)\omega_2^2 + (\phi_4-\phi_2)\omega_1^2\right]s^2$$

when $s = j\omega$

$$\begin{aligned}\Delta_N &= \left[(\phi_3-\phi_1) + (\phi_4-\phi_2)\right]\omega^4 - \left[(\phi_3-\phi_1)\omega_2^2 + (\phi_4-\phi_2)\omega_1^2\right]\omega^2 \\ &= (\phi_3-\phi_1)(\omega_4 - \omega_2^2\omega^2) + (\phi_4-\phi_2)(\omega_4 - \omega_1^2\omega^2)\end{aligned} \quad \text{(B-11)}$$

Using the expressions for resonant frequencies of $\omega_1(1+\Delta_1)$ and $\omega_2(1+\Delta_2)$ Equation (B-11) can be written as

$$\Delta_{N_1} = (1+3\Delta_1)\omega_2\omega_1^3(\phi_3-\phi_1)\left[\frac{\omega_1(1+\Delta_1)}{\omega_2} - \frac{\omega_2}{\omega_1(1+\Delta_1)}\right]$$

$$+ \omega_1\omega_1^3(1+3\Delta_1)(\phi_4-\phi_2)\left[\frac{\omega_1(1+\Delta_1)}{\omega_1} - \frac{\omega_1}{\omega_1(1+\Delta_1)}\right]$$

$$= \omega_2\omega_1^3(1+3\Delta_1)\left[(\phi_3-\phi_1)\left(\frac{\omega_1(1+\Delta_1)}{\omega_2} - \frac{\omega_2}{\omega_1(1+\Delta_1)}\right) + \frac{\omega_1}{\omega_2}(\phi_4-\phi_2)2\Delta_1\right]$$

In a similar fashion, Δ_{N_2} can be found:

$$\Delta_{N_2} = \omega_1\omega^3(\phi_3-\phi_1)\left(\frac{\omega^2\omega_2^2}{\omega\omega_1}\right) + \omega_1\omega^3(\phi_4-\phi_2)\left(\frac{\omega}{\omega_1} - \frac{\omega_1}{\omega}\right)$$

$$= \omega_1\omega_2^3(1+3\Delta_2)\left[(\phi_4-\phi_2)\left(\frac{\omega_2(1+\Delta_2)}{\omega_1} - \frac{\omega_1}{\omega_2(1+\Delta_2)}\right) + \frac{\omega_2}{\omega_1}(\phi_3-\phi_1)2\Delta_2\right]$$

Using the values for ω_1, ω_2, Δ_1, Δ_2, etc.,

$$\Delta_{N_1} = \omega_2\omega_1^3 \times 3.16$$

$$\Delta_{N_2} = \omega_1\omega_2^3 \times 0.782$$

Therefore, the magnitude of the resonant peaks can be calculated to be:

$$\frac{\Delta_{N_1}}{\Delta_{D_1}} = \frac{3.16}{2.335 \times 2\zeta} = 135.2 \quad \text{for } \zeta = 0.005$$

and

$$\frac{\Delta_{N_2}}{\Delta_{D_2}} = \frac{0.782}{2.035 \times 2\zeta} = 38.5 \quad \text{for } \zeta = 0.005$$

To summarize: The damping ratio assumed (0.005) results in amplitude ratios at resonances of

$$\left|\frac{\Delta_{N_1}}{\Delta_{D_1}}\right| = 135 \text{ and } \left|\frac{\Delta_{N_2}}{\Delta_{D_2}}\right| = 38.5$$

Because of the choice of ϕ_1 and ϕ_2, the transfer function $\Phi(s)$ has the form

$$\Phi(s) = -\frac{I_{xy}}{I_x} \frac{\left(-\frac{s^2}{194^2}+1\right)}{\left(\frac{s^2}{84^2}+1\right)\left(\frac{s^2}{215^2}+1\right)}$$

assuming negligible damping.

Separating this into two components

$$\Phi(s) = -\frac{I_{xy}}{I_x}\left[\frac{+1.40}{\frac{s^2}{84^2}+1} - \frac{0.40}{\frac{s^2}{215^2}+1}\right]$$

Thus the more complex equation for $\Phi(s)$ can be written to include the damping.

$$\Phi(s) = -\frac{I_{xy}}{I_x}\left[\frac{+1.40}{\frac{s^2}{84^2}+0.01\frac{s}{84}+1} - \frac{0.40}{\frac{s^2}{215^2}+0.01\frac{s}{215}+1}\right]$$

The approximations used in obtaining $\frac{\Delta_N}{\Delta_D}$ result in the difference between the two set of numbers, i.e., 1.35 as compared to 1.40, etc. If ζ_1 and ζ_2 were not the same and if ϕ_1 and ϕ_2 were less fortunately chosen, it would be necessary to obtain the peak amplitude ratio by the more complicated approximation technique above.

If the final $\Phi(s)$ transfer function is readjusted to have resonant peaks at 80 rad/sec and 214 rad/sec and a gain changing pair of zeros at ±194 rad/sec, the transfer function has the form

$$\Phi(s) = -\frac{\left(-\frac{s^2}{194^2}+1\right)\frac{I_{xy}}{I_x}}{\left(\frac{s^2}{80^2}+.01\frac{s}{80}+1\right)\left(\frac{s^2}{214^2}+.01\frac{s}{214}+1\right)}$$

This can be approximated by

$$\bar{\Phi}(s) = \frac{1.36\,\frac{I_{xy}}{I_x}}{\frac{s^2}{80^2} + 0.01\,\frac{s}{80} + 1} - \frac{0.36\,\frac{I_{xy}}{I_x}}{\frac{s^2}{214^2} + 0.01\,\frac{s}{214} + 1}$$

Any technique which is too sensitive to changes in the above $\bar{\Phi}(s)$ would <u>not</u> be a very logical approach to stabilizing the SAS system. Therefore, it is felt that the accuracy of approximation is not too critical and that precise knowledge of it should not be necessary for the scope of the analysis in which this data is employed.

APPENDIX C

ANALYSIS OF PRESSURE FEEDBACK STABILIZATION OF A HYDRAULIC ACTUATOR HAVING A RESONANT LOAD AND A FLEXIBLE SUPPORTING STRUCTURE

The equations for an actuator transfer function are derived on the basis that the device is a hydraulic boost actuator with mechanical command inputs determining the position of the cylinder. Fig. C-1 is a pictorial drawing of the servo configuration.

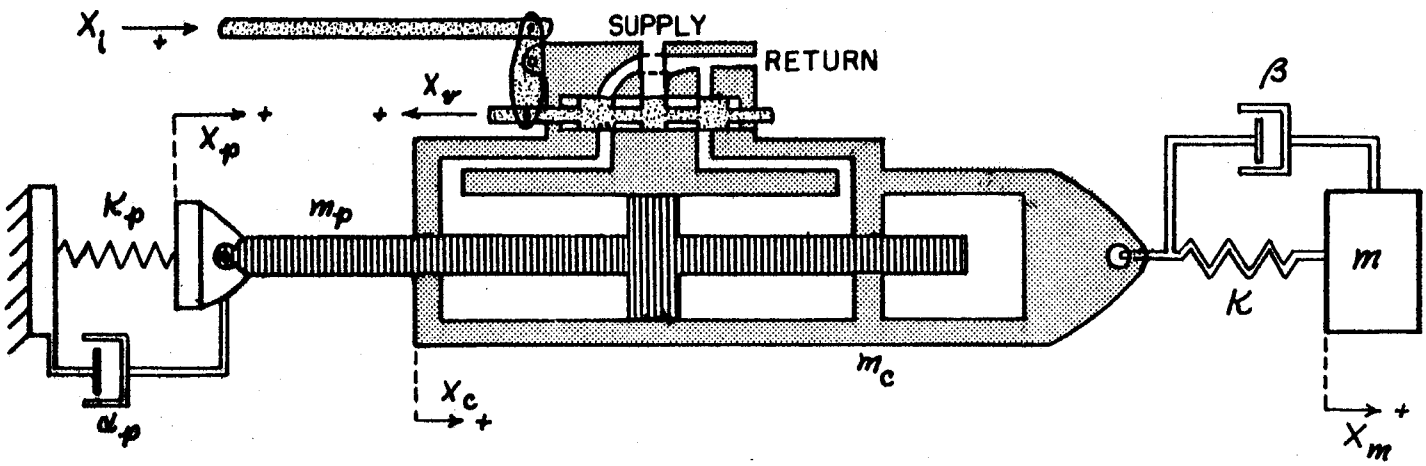

Figure C-1 Pictorial Diagram of Servo Actuator and Load

The schematic of the mechanical coupling is shown in Figure C-2.

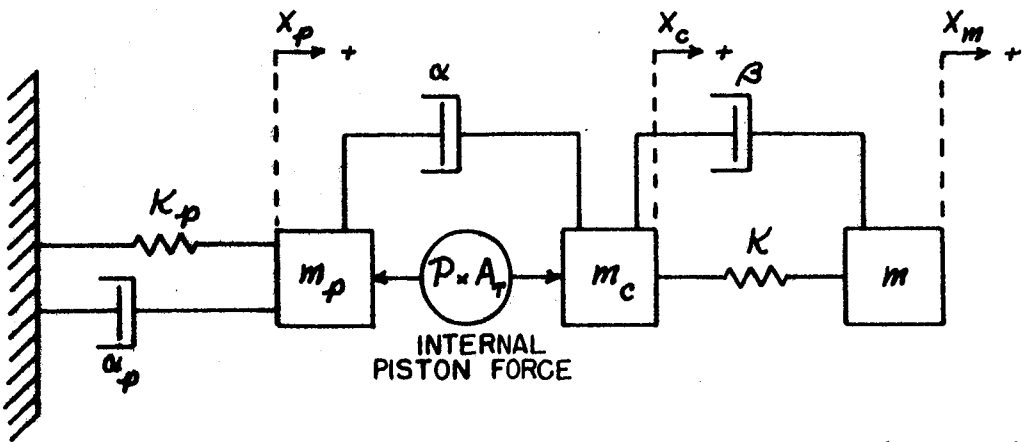

Figure C-2 Schematic of Mechanical Coupling of Servo Actuator

The equations of motion can then be determined by computing the acceleration on each mass.

$$m_p \ddot{X}_p = -K_p X_p - \alpha_p \dot{X}_p + \alpha\left(\dot{X}_c - \dot{X}_p\right) - PA_T \tag{C-1}$$

$$m_c \ddot{X}_c = PA_T - \alpha\left(\dot{X}_c - \dot{X}_p\right) - \beta\left(\dot{X}_c - \dot{X}_m\right) - K\left(X_c - X_m\right) \tag{C-2}$$

$$m\ddot{X}_m = \beta\left(\dot{X}_c - \dot{X}_m\right) + K\left(X_c - X_m\right) \tag{C-3}$$

These equations can be expressed in Laplace operation form and written as a matrix:

$$\begin{bmatrix} m_p S^2 + (\alpha + \alpha_p) S + K_p & -\alpha S & 0 \\ -\alpha S & m_c S^2 + (\alpha + \beta) S + K & -(\beta S + K) \\ 0 & -(\beta S + K) & m S^2 + \beta S + K \end{bmatrix} \begin{bmatrix} X_p \\ X_c \\ X_m \end{bmatrix} = \begin{bmatrix} -PA_T \\ +PA_T \\ 0 \end{bmatrix} \tag{C-4}$$

One can then solve for the various motions, e.g.

$$X_m = PA_T \frac{\begin{vmatrix} m_p S^2 + (\alpha + \alpha_p) S + K_p & -\alpha S & -1 \\ -\alpha S & m_c S^2 + (\alpha + \beta) S + K & +1 \\ 0 & -(\beta S + K) & 0 \end{vmatrix}}{\begin{vmatrix} m_p S^2 + (\alpha + \alpha_p) S + K_p & -\alpha S & 0 \\ -\alpha S & m_c S^2 + (\alpha + \beta) S + K & -(\beta S + K) \\ 0 & -(\beta S + K) & m S^2 + \beta S + K \end{vmatrix}} = PA_T \frac{|H|}{|D|} \tag{C-5}$$

where

$$|H| = \begin{vmatrix} m_p s^2 + \alpha_p s + K_p & -\alpha s & -1 \\ m_c s^2 + \beta s + K & m_c s^2 + (\alpha+\beta)s + K & +1 \\ -(\beta s + K) & -(\beta s + K) & 0 \end{vmatrix}$$

$$= -\begin{vmatrix} (m_p + m_c)s^2 + (\alpha_p + \beta)s + (K + K_p) & m_c s^2 + \beta s + K & 0 \\ m_c s^2 & m_c s^2 + \alpha s & +1 \\ +1 & +1 & 0 \end{vmatrix} (\beta s + K)$$

$$= +(\beta s + K)\left[-(m_c + m_p)s^2 - (\alpha_p + \beta)s - (K + K_p) - (ms^2 + \beta s + K)\right]$$

One must then construct a block diagram of the actuator showing how the various flow rates, etc., result in an output cylinder displacement.

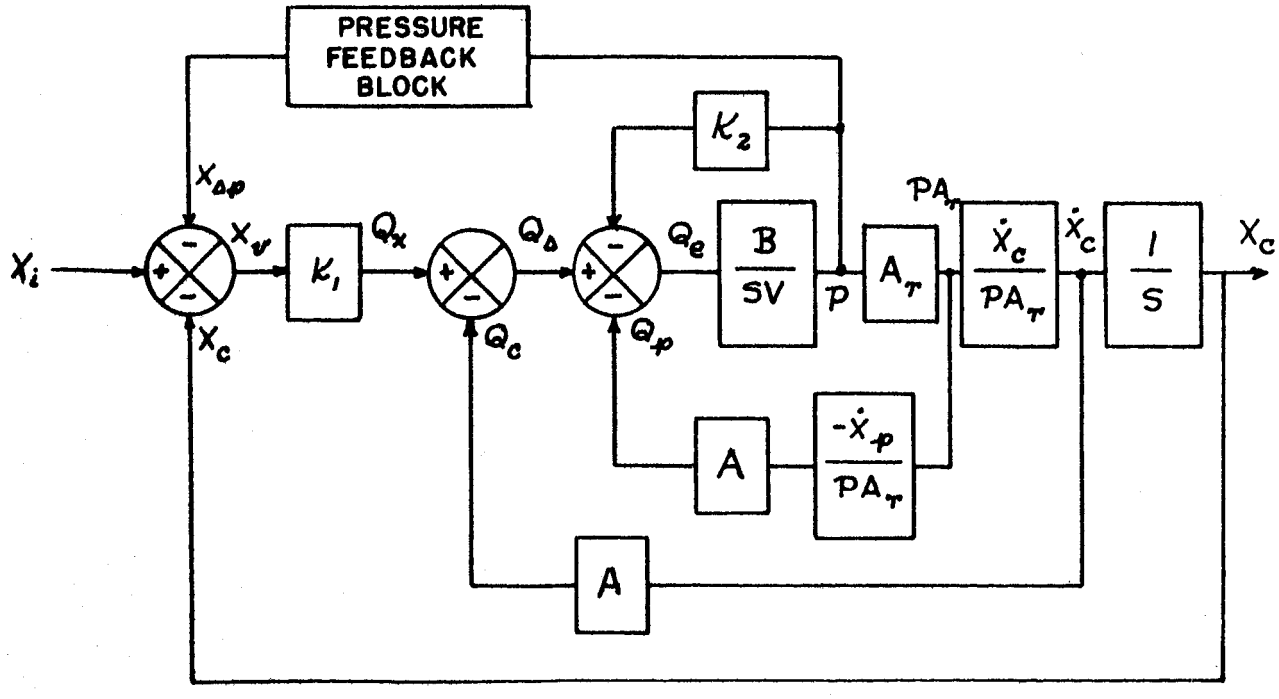

Figure C-3 Block Diagram of Servo Actuator and Load Interaction

where

X_i = input command position, ft

X_c = actuator output position, ft

$X_{\Delta p}$ = pressure feedback valve displacement, ft

X_v = actual valve displacement, ft

K_1 = flow rate / unit valve displacement, $ft^3/\frac{ft}{sec}$

Q_x = fluid flow rate into cylinder, ft^3/sec

Q_c = volumetric rate resulting from cylinder motion, ft^3/sec

Q_p = volumetric rate resulting from piston motion, ft^3/sec

Q_e = volumetric rate error which determines internal pressure ft^3/sec

A_T = total area of piston faces, ft^2

A = area of one piston face, ft^2

B = bulk modulus of fluid, lb/ft^2

V = volume of one chamber, ft^3

K_2 = leakage between chambers

The actuator equations resulting from this block diagram can be expressed as an X_c/X_i transfer function which includes the effect of the support structure motions on the valve displacement. For position errors where this cylinder displacement is measured relative to the piston, the effect of support flexibility is considerably less and these equations are not the correct ones. For that case, output would be $X_c - X_p$ for X_i input commands.

Let the pressure feedback block have the form

$$\frac{X_{\Delta p}}{p} = \frac{K_3 \tau_3 S}{\tau_3 S + 1}$$

and assume the leakage K_2 is negligible (any leakage also tends to provide damping

but the fluid flow losses severely limit this technique for stabilizing a servo piston).

One can therefore form the set of loop equations which will result in an expression for the over-all transfer function.

For ease of handling, let the various determinants be defined as:

$$|A| = \begin{vmatrix} m_p S^2+(\alpha+\alpha_p)S+K_p & -1 & 0 \\ -\alpha S & +1 & -(\beta S+K) \\ 0 & 0 & mS^2+\beta S+K \end{vmatrix} \qquad (C-6)$$

$$|B| = \begin{vmatrix} -\alpha S & -1 & 0 \\ m_c S^2+(\alpha+\beta)S+K & +1 & -(\beta S+K) \\ 1 \quad -(\beta S+K) & 0 & mS^2+\beta S+K \end{vmatrix} \qquad (C-7)$$

$$|D| = \begin{vmatrix} m_p S^2+(\alpha+\alpha_p)S+K_p & -\alpha S & 0 \\ -\alpha S & m_c S^2+(\alpha+\beta)S+K & -(\beta S+K) \\ 0 & -(\beta S+K) & mS^2+\beta S+K \end{vmatrix} \qquad (C-8)$$

$$|E| = |A| + |B| = \begin{vmatrix} m_p S^2+\alpha_p S+K_p & -1 & 0 \\ m_c S^2+\beta S+K & +1 & -(\beta S+K) \\ -(\beta S+K) & 0 & mS^2+\beta S+K \end{vmatrix} \qquad (C-9)$$

From the matrix expression (4), one can write expressions for X_c, X_p, $\dot{X}_c$, $\dot{X}_p$, etc.

$$X_c = PA_T \frac{|A|}{|D|} \qquad \dot{X}_c = PA_T S \frac{|A|}{|D|} \tag{C-10}$$

$$-X_p = PA_T \frac{|B|}{|D|} \qquad -\dot{X}_p = PA_T S \frac{|B|}{|D|} \tag{C-11}$$

$$\dot{X}_c - \dot{X}_p = PA_T S \frac{|E|}{|D|} \tag{C-12}$$

From the block diagram (Fig. C-3) one can write

$$\frac{\dot{X}_c}{Q_e} = \frac{BA_T}{V} \frac{|A|}{|D|} \tag{C-13}$$

$$\frac{PA_T}{Q_\Delta} = \frac{\frac{BA_T}{SV}}{1 + \frac{BAA_T}{V} \frac{|B|}{|D|}} \tag{C-14}$$

Then combining (10) and (14)

$$\frac{\dot{X}_c}{Q_\Delta} = \frac{\dot{X}_c}{PA_T} \cdot \frac{PA_T}{Q_\Delta} = \frac{\frac{BA_T}{V} \frac{|A|}{|D|}}{1 + \frac{BAA_T}{V} \frac{|B|}{|D|}} \tag{C-15}$$

but since $$\frac{\dot{X}_c}{Q_x} = \frac{\frac{\dot{X}_c}{Q_\Delta}}{1 + A\,\frac{\dot{X}_c}{Q_\Delta}}$$

thus

$$\frac{\dot{X}_c}{Q_x} = \frac{\frac{BA_T}{V}\,\frac{|A|}{|D|}}{1 + \frac{BAA_T}{V}\left(\frac{|A|}{|D|} + \frac{|B|}{|D|}\right)} = \frac{\frac{BA_T}{V}\,\frac{|A|}{|D|}}{1 + \frac{BAA_T}{V}\,\frac{|E|}{|D|}} \qquad \text{(C-16)}$$

therefore

$$\frac{X_c}{X_v} = \frac{\frac{1}{S}\,\dot{X}_c}{\frac{1}{K_1}\,Q_x} = \frac{\frac{K_1 BA_T}{SV}\,\frac{|A|}{|D|}}{1 + \frac{BAA_T}{V}\,\frac{|E|}{|D|}} \qquad \text{(C-17)}$$

Also, from Figure 3, one finds that

$$\frac{P}{Q_x} = \frac{\dot{X}_c}{Q_x} \cdot \frac{1}{\frac{\dot{X}_c}{PA_T}} \cdot \frac{1}{A_T} = \frac{\frac{BA_T}{V}\,\frac{|A|}{|D|}}{1 + \frac{BAA_T}{V}\,\frac{|E|}{|D|}} \cdot \frac{1}{A_T S\,\frac{|A|}{|D|}}$$

$$\therefore \quad \frac{P}{Q_x} = \frac{\frac{B}{SV}}{1 + \frac{BAA_T}{V}\,\frac{|E|}{|D|}} \qquad \text{(C-18)}$$

since $$\frac{P}{X_v} = \frac{K_1 P}{Q_x}, \quad P = X_v \left[\frac{\frac{K_1 B}{SV}}{1 + \frac{BAA_T}{V}\,\frac{|E|}{|D|}}\right] \qquad \text{(C-19)}$$

the pressure feedback is expressed as

$$X_{\Delta p} = \left(\frac{\tau_3 K_3 S}{\tau_3 S+1}\right) P = \left(\frac{\tau_3 K_3 S}{\tau_3 S+1}\right)\left(\frac{\frac{K_1 B}{SV}}{1+\frac{BAA_T}{V}\frac{|E|}{|D|}}\right) X_v \qquad \text{(C-20)}$$

The valve position is expressed by the equation

$$X_v = X_i - X_{\Delta p} - X_c \qquad \text{(C-21)}$$

which results in the equation

$$\frac{X_c}{X_i} = \frac{\frac{X_c}{X_v}}{1+\frac{X_{\Delta p}}{X_v}+\frac{X_c}{X_v}} \qquad \text{(C-22)}$$

Equations (17), (20), and (22) result in the over-all actuator transfer function:

$$\frac{X_c}{X_i} = \frac{\frac{K_1 B A_T}{SV}\frac{|A|}{|D|}}{1+\frac{BAA_T}{V}\frac{|E|}{|D|}+\frac{B\tau_3 K_1 K_3}{V(\tau_3 S+1)}+\frac{BK_1 A_T}{SV}\frac{|A|}{|D|}} \qquad \text{(C-23)}$$

If equation (23) is expanded, it becomes an "algebraic nightmare" and is impossible to analyze. It therefore becomes necessary to analyze (23) in its present form by "dismembering" it to exhibit the effect of $\frac{B}{V}$, K_3, τ_3, α, K_1 etc. on the final $\frac{X_c}{X_i}$ transfer function.

Setting the denominator of equation (23) = 0 exhibits the roots of the characteristic equation. These roots are the poles of the $\frac{X_c}{X_i}$ transfer function.

They are also the poles of the transfer function expressing the reaction force of the load on the actuator $\frac{S^2 m X_m}{X_i}$

$$1 + \frac{BAA_T}{V}\frac{|E|}{|D|} + \frac{K_1 BA_T}{SV}\frac{|A|}{|D|} + \frac{B\tau_3 K_1 K_3}{V(\tau_3 S+1)} = 0 \qquad \text{(C-24)}$$

By factoring, (24) can be written as

$$1 + \frac{B}{V}\frac{AA_T}{\frac{|D|}{|E|}}\left\{1 + \frac{\frac{K_1}{A}}{\frac{S|E|}{|A|}}\left(1 + \frac{\frac{\tau_3 K_3}{A_T}S|D|}{(\tau_3 S+1)|A|}\right)\right\} = 0 \qquad \text{(C-25)}$$

Therefore, for large $\frac{B}{V}$, $\left(\frac{B}{V} \gg \frac{1}{AA_T}\right)$ (25) reduces to

$$1 + \frac{\frac{K_1}{A}}{\frac{S|E|}{}}\left[\frac{|A| + \tau_3 S\left(\frac{K_3}{A_T}|D| + |A|\right)}{(\tau_3 S+1)}\right] = 0 \qquad \text{(C-26)}$$

This is a valid approximation for hydraulic systems since the effect of $\frac{B}{V}$ on the roots of the characteristic equation is very small. This has been determined analytically by the writer using root locus techniques similar to the ones discussed in later portions of this analysis. Pneumatic servos having small $\frac{B}{V}$ obviously cannot make this approximation.

If there is no pressure feedback, (26) reduces to

$$1 + \frac{\frac{K_1}{A}|A|}{S|E|} = 0 \qquad \text{(C-27)}$$

Expanded, (27) becomes

$$1+\frac{\frac{K_1}{A}\begin{vmatrix} m_p s^2+\alpha_p s+K_p & 0 & -(\beta s+K) \\ -\alpha s & +1 & -(\beta s+K) \\ 0 & 0 & ms^2+\beta s+K \end{vmatrix}}{s\begin{vmatrix} (m_c+m_p)s^2+(\beta+\alpha_p)s+(K+K_p) & 0 & -(\beta s+K) \\ m_c s^2+\beta s+K & +1 & -(\beta s+K) \\ -(\beta s+K) & 0 & ms^2+\beta s+K \end{vmatrix}}$$

which results in an equation of the form

$$1+\frac{\frac{K_1}{A}(m_p s^2+\alpha_p s+K_p)(ms^2+\beta s+K)}{s\left\{\left[(m_c+m_p)s^2+(\beta+\alpha_p)s+(K+K_p)\right](ms^2+\beta s+K)-(\beta s+K)^2\right\}}=0 \qquad \text{(C-27)}$$

for the expression for the roots of the characteristic equation of $\frac{x_c}{x_i}$ as a function of valve gain $\frac{K_1}{A}$.

The term $-(\beta s+K)^2$ in equation (27) has very little effect on the roots resulting from $\left[\quad\right]$ for values of $K_p \geq K$ and $m_p, m_c \ll m$.

The major influence is to lower the value of the roots of $(ms^2+\beta s+K)$. For typical values of m, β, K, etc., the natural radian frequency, ω_n, of the resulting poles becomes

$$\omega_n = \sqrt{\frac{K}{m}} \times \sqrt{\frac{K_p}{K+K_p}}$$

which is the expression for two springs in series.

The damping is increased only slightly for the β, m, K, etc., values which are being considered in this analysis.

If, for example, we assume $K_p = 4K$ and α_p is such that $\zeta_p = 0.2$, then

for the X-15, representative values would be

$\alpha_p = 2\zeta_p m_p \omega_p = 488$ $\qquad \omega_p = \sqrt{1.49 \times 10^6} = 1220$ rad/sec

$K_p = 1.49 \times 10^6$ $\qquad \omega_m = 89$ rad/sec

$K = 0.372 \times 10^7$ $\qquad m_c = m_p = 1$ slug (assumed)

$m = 47$ slugs

$\beta = 83.6$ (for $\zeta = 0.01$)

Therefore, equation (27) becomes

$$0 = 1 + \frac{\frac{K_1}{A}\left(S^2+488S+1.49\times10^6\right)\left(47S^2+83.6S+0.372\times10^6\right)}{S\left[\left(25S^2+571.6S+1.86\times10^6\right)\left(47S^2+83.6S+0.372\times10^6\right)-\left(83.6S+0.372\times10^6\right)^2\right]}$$

This can be reduced to

$$0 = 1 + \frac{\frac{K_1}{A}\left(\frac{S^2}{1220^2}+0.40\frac{S}{1220}\right)\left(\frac{S^2}{89^2}+0.02\frac{S}{89}+1\right)}{S\left[1.25\left(\frac{S^2}{964.3^2}+0.297\frac{S}{964.3}+1\right)\left(\frac{S^2}{89^2}+0.02\frac{S}{89}+1\right)-.25\left(\frac{S}{4450}+1\right)\right]}$$

A subsidiary root locus of the denominator or a simple solution of the fourth order equation resulting from the combined terms results in the characteristic equation having the following form:

$$0 = 1 + \frac{\frac{K_1}{A}\left(\frac{S^2}{1220^2}+0.40\frac{S}{1220}+1\right)\left(\frac{S^2}{89^2}+0.02\frac{S}{89}+1\right)}{S\left(\frac{S^2}{964.3^2}+0.297\frac{S}{964.3}+1\right)\left(\frac{S^2}{80^2}+0.032\frac{S}{80}+1\right)}$$

For values of $\frac{K_1}{A} = 30$ (the valve gain of the X-15 actuator), the closed loop roots are

$S = -55$
$S = +3 \pm j83.1$
$S = -143 \pm j953$
} Poles (functions of $\frac{K_1}{A}$)

$S = -0.89 \pm j89$
$S = -244 \pm j1120$
} Zeros (fixed)

Since this is a description of an unstable actuator, it is obvious that the valve gain existing in the X-15 is reduced in this loop (i.e., the flexibility, etc. of the supports are not sensed by the valve because of the hysteresis and valve friction in the present system). If some of this hysteresis, etc. is reduced, the present X-15 power actuator is observed to be unstable. Since it is extremely difficult to assign a linear gain to this situation, it will only serve to show how the actuator frequency response would appear to be if the gain was reduced to a value where the roots are stable. This low gain would drastically reduce the actuator frequency response. Since it is interesting to find the phase shift in the 20 - 40 rad/sec region resulting from this actuator model, a simple phase angle solution was made ignoring the effect of the low frequency real pole. The contribution to the total phase lag due to roots at the 80 rad/sec region was less than 2° lag to 40 rad/sec. This is a negligible term. It is therefore realistic to ignore the phase effects of the structural roots when considering the residual oscillation problem.

If pressure feedback of the type shown in the block diagram (Figure C-3). is included, the position of the zeros of the numerator of (26) is modified in such a manner to increase the damping of the roots of the characteristic equation.

These zeros are located at the roots of

$$0 = 1 + \frac{\frac{\tau_3 K_3}{A_7} S|D|}{|A|(\tau_3 S+1)} \qquad \text{(C-28)}$$

Let

$$|F| = \begin{vmatrix} m_p S^2 + \alpha_p S + K_p & 0 & 0 \\ m_c S^2 + \beta S + K & m_c & -(\beta S + K) \\ -(\beta S + K) & m & mS^2 + \beta S + K \end{vmatrix}$$

and

$$|G| = \begin{vmatrix} m_p S^2 + \alpha_p S + K_p & -1 & 0 \\ m_c S^2 + \beta S + K & +1 & -(\beta S + K) \\ -(\beta S + K) & 0 & mS^2 + \beta S + K \end{vmatrix}$$

It can be shown that

$$|D| = S^2 |F| + \alpha S |G|$$

Thus, (28) can be written as

$$0 = 1 + \frac{\frac{\tau_3 K_3}{A_T} \left[S |F| + \alpha |G| \right] S^2}{(\tau_3 S + 1) |A|} \qquad \text{(C-29)}$$

The position of some of the zeros of (29) is a function of α. This dependence on α is exhibited by a subsidiary root locus of

$$0 = S |F| + \alpha |G|$$

or

$$0 = 1 + \frac{\alpha |G|}{S |F|} \qquad \text{(C-30)}$$

Expanding (30)

$$0 = 1 + \frac{\alpha \begin{vmatrix} (m_p+m_c)s^2+(\alpha_p+\beta)s+(K+K_p) & 0 & -(\beta s+K) \\ m_c s^2+\beta s+K & & -(\beta s+K) \\ -(\beta s+K) & & m s^2+\beta s+K \end{vmatrix}}{s \begin{vmatrix} m_p s^2+\alpha_p s+K_p & 0 & 0 \\ m_c s^2+\beta s+K & m_c & -(\beta s+K) \\ -(\beta s+K) & m & m s^2+\beta s+K \end{vmatrix}}$$

$$0 = 1 + \frac{\alpha\left\{\left[(m_p+m_c)s^2+(\alpha_p+\beta)s+(K+K_p)\right](m s^2+\beta s+K)-(\beta s+K)^2\right\}}{s\left\{(m_p s^2+\alpha_p s+K_p)\left[m_c(m s^2+\beta s+K)+m(\beta s+K)\right]\right\}}$$

This reduces to

$$0 = 1 + \frac{\frac{\alpha}{m+m_c}\left\{\left[\left(\frac{m_p+m_c}{K+K_p}\right)s^2+\left(\frac{\alpha_p+\beta}{K+K_p}\right)s+1\right]\left(\frac{m}{K}s^2+\frac{\beta}{K}s+1\right)\left(\frac{K+K_p}{K}\right)-\frac{K}{K_p}\left(\frac{\beta}{K}s+1\right)^2\right\}}{s\left\{\left(\frac{m_p}{K_p}s^2+\frac{\alpha_p}{K_p}s+1\right)\left(\frac{m m_c}{(m+m_c)K}s^2+\frac{\beta}{K}s+1\right)\right\}} \quad \text{(C-31)}$$

where $\frac{\alpha}{m+m_c}$ determines the closeness of the roots of (30) to the roots of $|G|$.

This locus determines the limitations of the pressure feedback. Large values of α reduce the effectiveness of the pressure feedback for stabilizing the actuator-load combination.

For the actuator in the X-15, α is approximately 4200 lb/ $\frac{\text{ft}}{\text{sec}}$. Therefore,

$\frac{\alpha}{m+m_c}$ = 87.5 and the roots of (30) can be evaluated by a root locus plot of (31). Using the m, K, etc. values in the example above, (31) becomes:

$$0 = 1 + \frac{87.5\left(\frac{s^2}{964.3^2} + 0.297\frac{s}{964.3} + 1\right)\left(\frac{s^2}{80^2} + 0.32\frac{s}{80} + 1\right)}{s\left(\frac{s^2}{1220^2} + 0.40\frac{s}{1220} + 1\right)\left(\frac{s^2}{616^2} + 0.1388\frac{s}{616} + 1\right)}$$

or

$$\frac{\alpha\left(\frac{s^2}{964.3^2} + 0.297\frac{s}{964.3} + 1\right)\left(\frac{s^2}{80^2} + 0.32\frac{s}{80} + 1\right)}{s\left(\frac{s^2}{1220^2} + 0.40\frac{s}{1220} + 1\right)\left(\frac{s^2}{616^2} + 0.1388\frac{s}{616} + 1\right)} = -48 \qquad \text{(C-32)}$$

Figure C-4 is a root locus plot of (C-32).

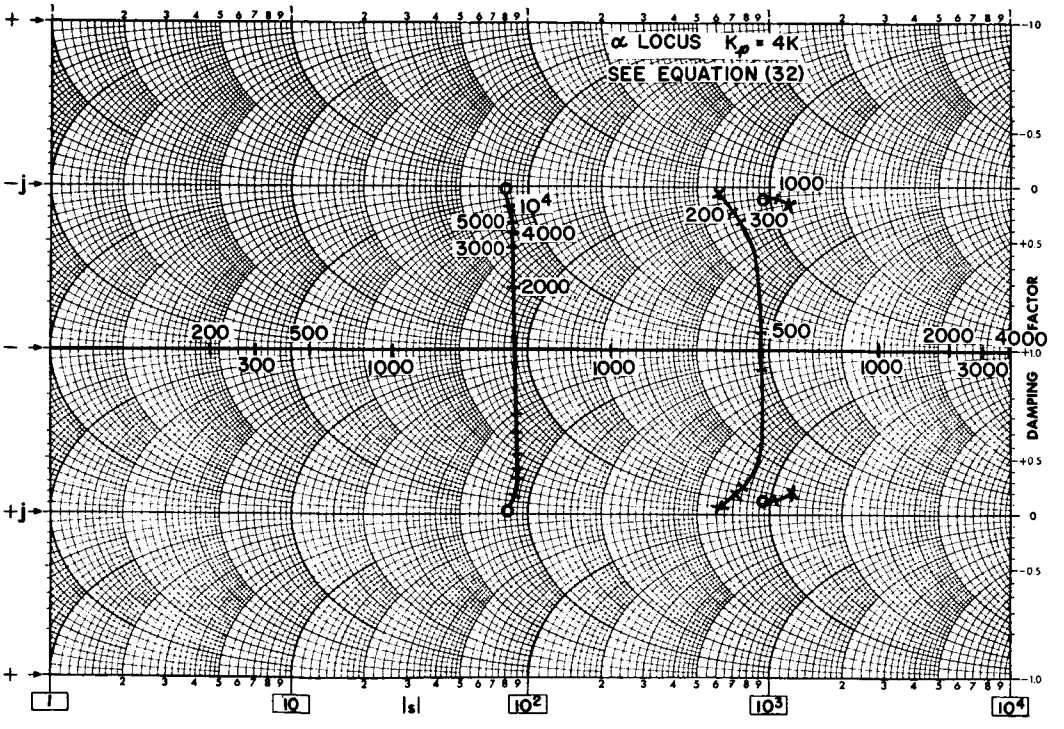

Figure C-4 Root Locus of Equation C-32 for α Variations

For α = 4200, these roots are approximately

$$-35 \pm j75 \,, \quad (-10,000 +)$$

and $\quad -143.5 \pm j953$

The roots resulting from the resonant load have been moved to a frequency and damping of ω_n = 78 and ζ = 0.448. This is the limiting value of damping that pressure feedback will be able to provide for the amount of internal actuator friction α which was assumed. The root locus of (32) also shows the improvement possible if α can be kept low.

Returning to equation (29), restated here,

$$0 = 1 + \frac{\frac{\tau_3 K_3}{A_T}\left(S|F| + \alpha|G|\right)S^2}{(\tau_3 S+1)|A|} \qquad \text{(C-29)}$$

one must analyze the effect of K_3 and τ_3 on the root locati ns of (29), given the values of the most predominant roots of $S|F|+\alpha|G|$.

As $S \rightarrow 0$, (29) becomes

$$0 = 1 + \frac{\tau_3 K_3}{A_T} S^2 \frac{\alpha K_p K}{K_p K}$$

$$= 1 + \frac{\tau_3 K_3 \alpha}{A_T} S^2$$

Thus (29) can be written as

$$0 = 1 + \frac{\frac{\tau_3 K_3}{A_T} S^2 \left(\frac{S^2}{78^2} + .896\,\frac{S}{78} + 1\right)\left(\frac{S^2}{964.3^2} + 0.297\,\frac{S}{964.3} + 1\right)\left(\frac{S}{10,000} + 1\right)}{(\tau_3 S+1)|A|\frac{1}{K K_p}} \qquad \text{(C-33)}$$

Equation (33) can be rewritten to determine the effect of K_3 and τ_3 separately:

$$0 = \tau_3 \left[\frac{1}{KK_p}|A| + \frac{K_3\alpha}{A_T} S\left(\frac{S}{78^2} + 0.896\,\frac{S}{78} + 1\right)\left(\frac{S^2}{964.3^2} + 0.297\,\frac{S}{964.3} + 1\right)\right] S + \frac{1}{KK_p}|A| \qquad \text{(C-34)}$$

The term in the square brackets approaches

$$\frac{K_3\alpha}{A_T} S\left(\frac{S^2}{78^2} + 0.896\,\frac{S}{78} + 1\right)\left(\frac{S^2}{964.3^2} + 0.297\,\frac{S}{964.3} + 1\right)$$

for large K_3. This is not too desirable because of the root at $S \approx 0$ which would result in low actuator frequency.

By a root locus plot of the term in square brackets in equation (34), Fig. C-5 one finds that no appreciable increase in damping of the structural roots is obtained for $K_3 > 10^{-6}$. Reasonable values of K_3 lie in the range 1×10^{-6} to 2.7×10^{-6}. The best balance between the position of the real root and structural damping for the problem being considered is about $K_3 = 1.3 \times 10^{-6}$. In more common units, this is a valve displacement of 0.0225 in./psi differential. Acceptable values would lie between 0.0173 in. to 0.061 in./psi.

For $K_3 = 1.3 \times 10^{-6}$, the root locations of the terms in the square brackets in equation (34) become

$S = -32$

$S = -30 \pm j57$ ($\omega = 64.5$, $\zeta = 0.465$)

$S = -143 \pm j954$ ($\omega = 964.3$, $\zeta = 0.1485$)

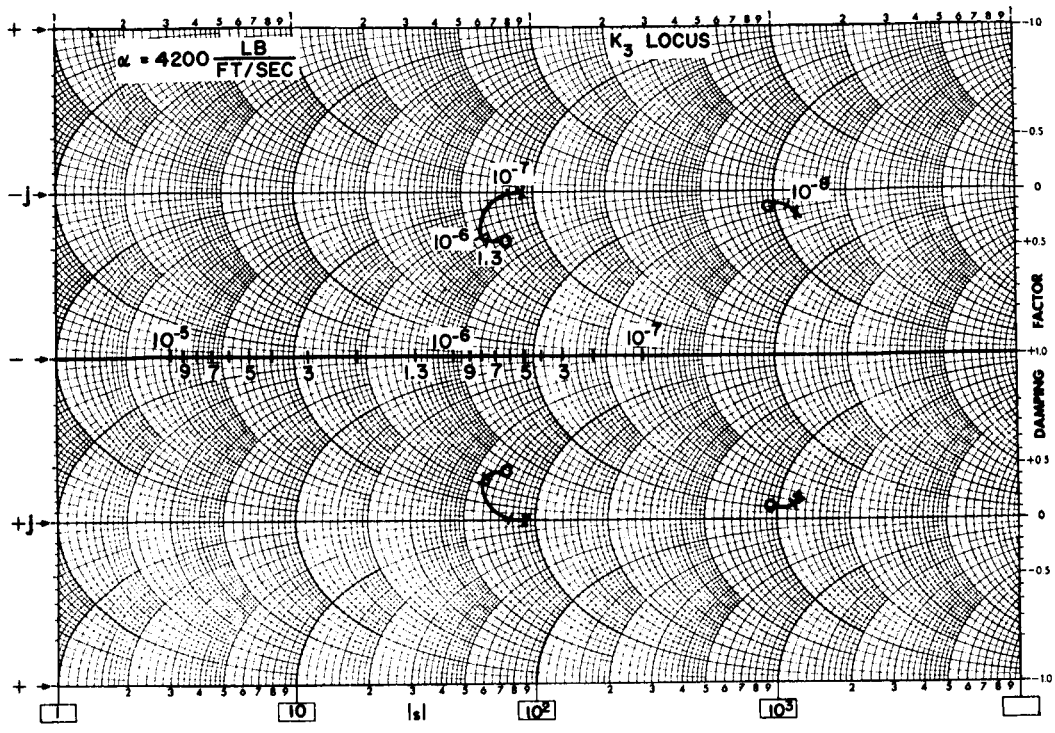

Figure C-5 Root Locus of Equation C-34 for K_3 Variations

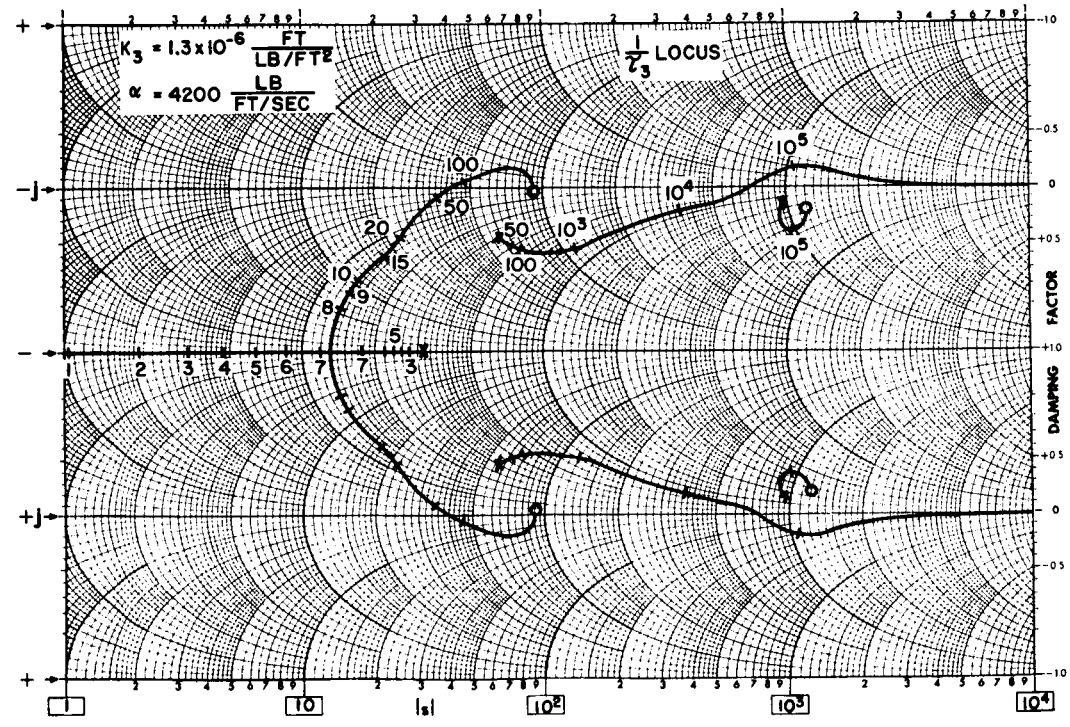

Figure C-6 Root Locus of Equation C-34 for τ_3 Variations

Thus equation (34), for the selected value of K_3, reduces to

$$0 = \tau_3 S\left(\frac{S}{32}+1\right)\left(\frac{S^2}{64.5^2}+0.93\,\frac{S}{64.5}+1\right)\left(\frac{S^2}{964.3^2}+0.297\,\frac{S}{964.3}+1\right)+\frac{1}{KK_p}|A| \qquad \text{(C-35)}$$

This can be restated as a root locus problem in $1/\tau_3$. The root positions of (35) as a function of $1/\tau_3$ are plotted in Figure C-6.

The most significant result of the locus is that the roots at $S = 0$ and $S = -32$ combine and then cross the imaginary axis at $S = \pm j40$. Intermediate values of $1/\tau_3$ result in roots exhibiting good damping and sufficiently high frequency to result in very acceptable actuator response characteristics.

The most ideal range of $1/\tau_3$ is not too obvious from this root locus. The high-pass characteristics most effective are between 5 and 100, since $1/\tau_3 < 5$ would produce low actuator response and a $1/\tau_3 > 100$ would possibly produce unstable roots.

Since the optimum value of $1/\tau_3$ is unknown, values of 5, 15 and 50 are used as examples in the following analysis.

One can now solve the $\frac{K_1}{A}$ root locus problem posed in equation (26). Substitution of the values determined in Fig. C-6, equation (26) becomes, for the $1/\tau_3 = 15$ case

$$0 = 1 + \frac{\frac{K_1}{A}\left(\frac{S^2}{22^2}+1.21\,\frac{S}{22}+1\right)\left(\frac{S^2}{66.7^2}+0.99\,\frac{S}{66.7}+1\right)}{S\left(\frac{S^2}{80^2}+0.32\,\frac{S}{80}+1\right)\left(\tau_3 S+1\right)} \qquad \text{(C-36)}$$

Figures C-7, C-8 and C-9 are the root locus plots of (36) for $1/\tau_3$ of 5, 15 and 50. The present actuator on the X-15 has a valve gain, K_1/A, of 30. It is important to note that pressure feedback stabilization with gains much less than 10 is not too effective. For gains of the order of 20 to 50, the actuator exhibits good frequency response with no undamped roots and a relatively wide bandwidth. Since the actuator phase lag is a major factor in the amplitude of the residual oscillation resulting from hysteresis and dead band non-linearities, it would be advantageous to have this higher actuator frequency response and consequent smaller phase lags.

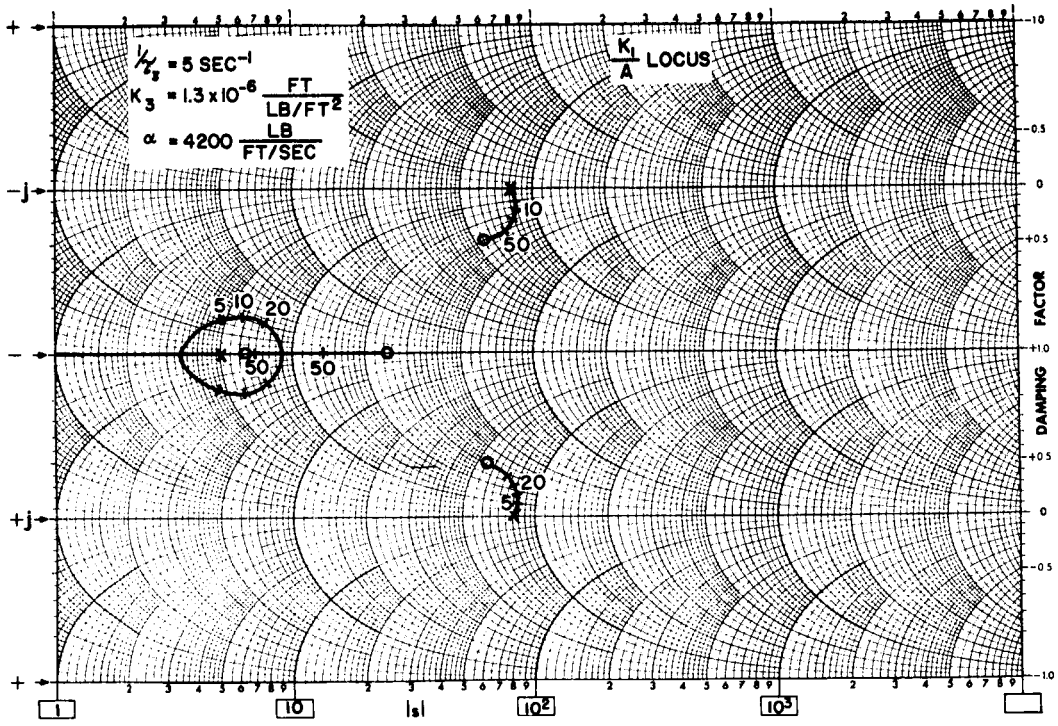

Figure C-7 Root Locus of Equation C-36 for $\tau_3^{-1} = 5$ and K_1 Changes

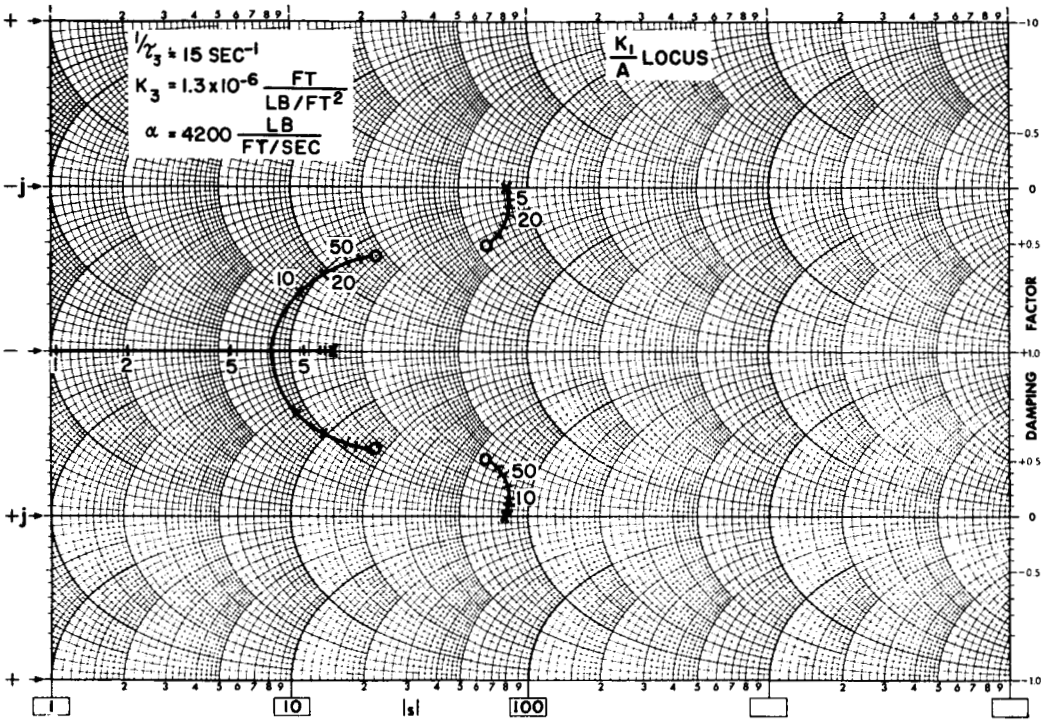

Figure C-8 Root Locus of Equation C-36 for $\tau_3^{-1} = 15$ and K_1 Changes

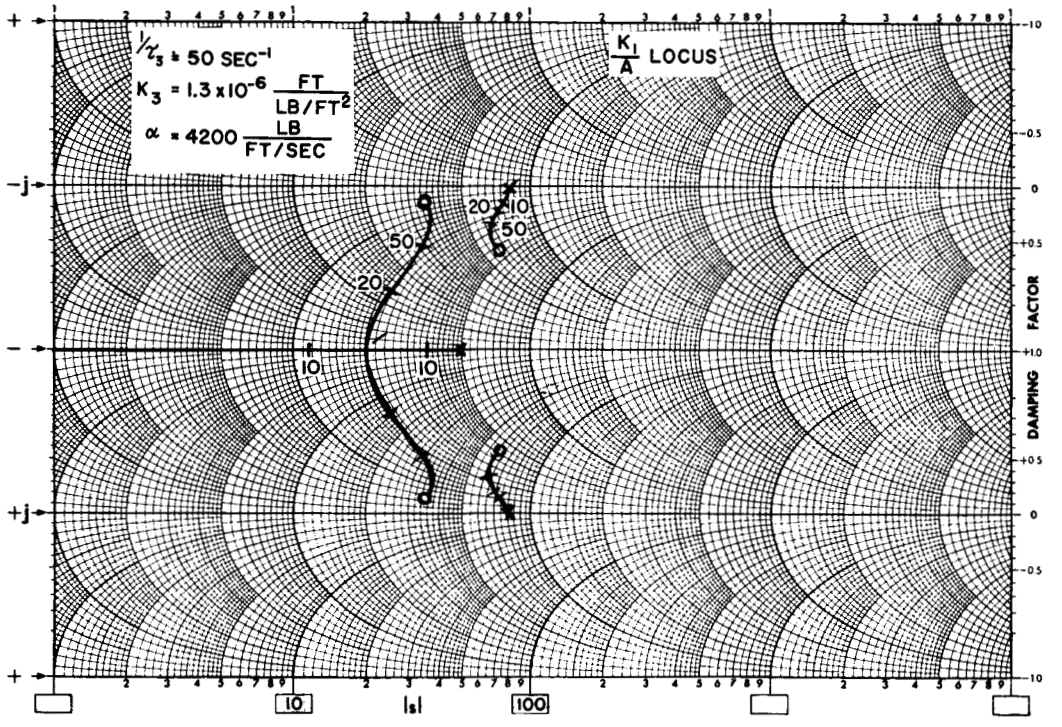

Figure C-9 Root Locus of Equation C-36 for $\tau_3^{-1} = 50$ and K_1 Changes

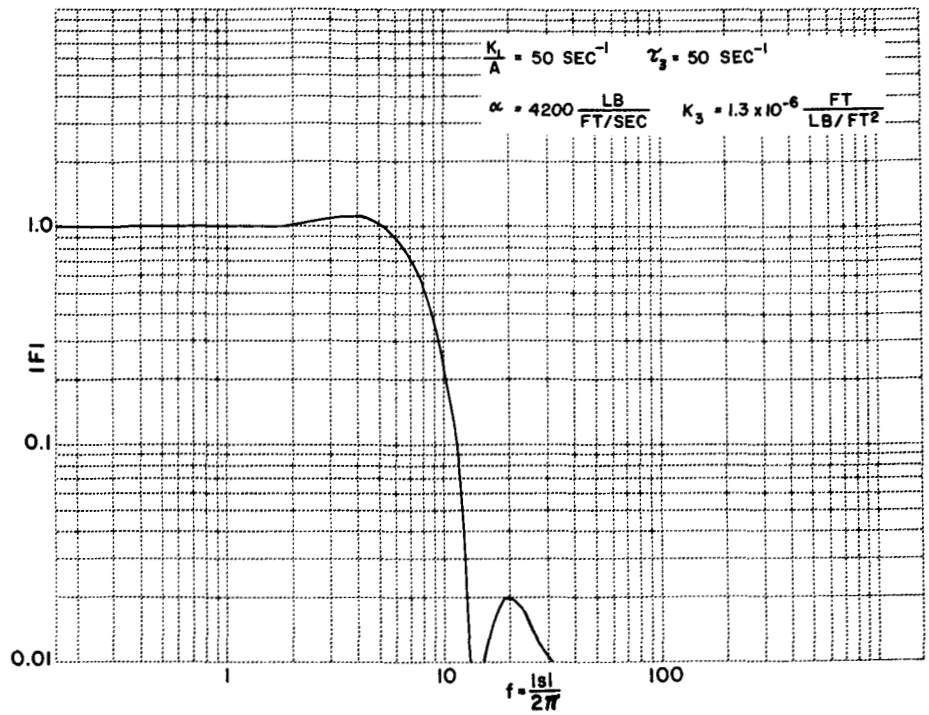

Figure C-10 Amplitude Ratio vs. Frequency of Servo Actuator for Selected Values of K_1/A, τ_3 and K_3

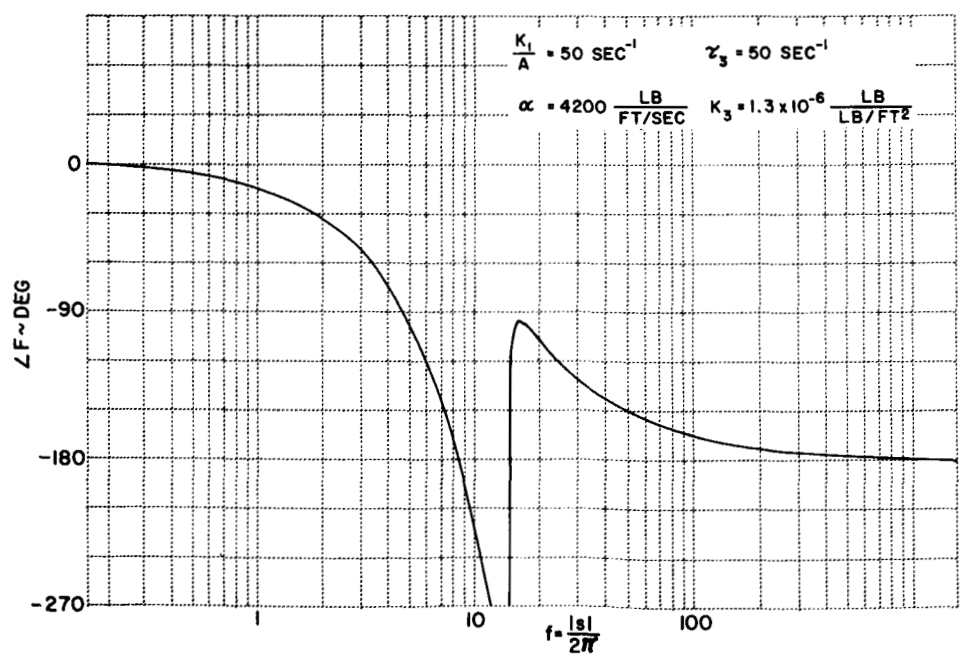

Figure C-11 Phase Angle vs. Frequency of Servo Actuator for Selected Values of K_1/A, τ_3 and K_3

Figures C-10 and C-11 are amplitude ratio and phase angle plots of the best case obtained in this analysis.

The major advantages of pressure feedback can be listed as:

a. Resonant loads on the actuator are damped by the pressure feedback loop.
b. Higher valve gains can be employed to increase actuator frequency response.
c. The control system hysteresis and dead band which exist in the present system and tend to stabilize or at least reduce the tendency for the structural oscillation to be excited can be reduced. This will reduce the low frequency residual oscillation amplitude without making the system unstable at the high frequency mode.
d. Servo piston support flexibility and bulk modulus effects which are destabilizing are readily compensated for by pressure feedback.
e. The reaction force transfer function (of the load back to the piston) has the same characteristic equation as the output/input displacement transfer function. Therefore, there are no structural resonance roots to make the **SAS** system unstable for the necessary **SAS** loop gains.

APPENDIX D

CALCULATION OF THE CLOSED LOOP STABILITY CHARACTERISTICS OF THE SAS SYSTEM EMPLOYING A PRESSURE FEEDBACK STABILIZED ACTUATOR

At $q = 0$ and for low frequencies where the surface is a rigid unit, the roll acceleration, $\ddot{\phi}$, resulting from a horizontal stabilizer angular acceleration is proportional to the ratio of the product of inertia about the horizontal stabilizer spindle axis and the moment of inertia of the fuselage. This is symbolically stated as

$$\left.\frac{\ddot{\phi}}{\ddot{\delta}_A}\right|_{\omega \to 0} = \frac{I_{xy}}{I_x} \tag{D-1}$$

where the I_{xy} and I_x are the rigid body values. As the frequency of δ_A increases the effective I_{xy} changes because elements of the surface are moving at rates different than the same elements of the rigid body would. This increase in the effective coupling can be approximated by a transfer function of the form

$$\frac{\ddot{\phi}}{\delta_A} = \frac{S^2 \frac{I_{xy}}{I_x}}{\frac{S^2}{\omega_n^2} + 2\zeta \frac{S}{\omega_n} + 1} \tag{D-2}$$

ω_n is the frequency at which the surface resonates and ζ is the damping ratio. This is not an exact representation for two major reasons:

1. The value of I_{xy} changes with frequency in a different manner than the lumped constant picture that this expression describes.
2. The roll mode of the fuselage couples with the surface motion to produce a different transfer function.

A more exact approximation for the coupling between δ_A and ϕ (ignoring for this discussion higher frequency modes) could be expressed as

$$\frac{\ddot{\phi}}{\delta_A} = \frac{S^2 K_S \frac{I_{xy}}{I_x}}{\frac{S^2}{\omega_n^2} + 2\zeta \frac{S}{\omega_n} + 1} \tag{D-3}$$

where the K_s is a factor to approximate more accurately the coupling term. It is unlikely for any study of the horizontal surface that K_s would be outside the range $1 < K_s < 2$.

The actuator or surface output transfer function as a function of input command angle, δ_A / δ_{A_c}, can be considered to be the same as the X_c/X_i transfer function derived in Appendix C, since the scale factor for both is the same, and they are otherwise analogous of each other.

Thus one is able to form a reasonably close representation of the transfer function for low q conditions.

$$\frac{\ddot{\phi}}{\delta_{A_c}} = \frac{\ddot{\phi}}{\delta_A} \cdot \frac{\delta_A}{\delta_{A_c}} = \frac{\dot{\phi}}{\delta_A} \cdot \frac{X_c}{X_i} \tag{D-4}$$

$$= \frac{S^2 \frac{I_{XY}}{I_X} K_s}{\frac{S^2}{\omega_n^2} + 2\zeta \frac{S}{\omega_n} + 1} \; \frac{\frac{K_1}{A} \frac{|A|}{|D|}}{\frac{VS}{BAA_\pi} + S \frac{|E|}{|D|} + \frac{\tau_3 (K_1/A)(K_3/A_\pi)}{\tau_3 S + 1} + \frac{K_1}{A} \frac{|A|}{|D|}} \tag{D-5}$$

This reduces to, for an actuator employing pressure feedback:

$$\frac{\ddot{\phi}}{\delta_{A_c}} = \frac{K_s \frac{I_{XY}}{I_X} S^2 \left(\frac{\beta}{K} S + 1 \right)}{\left(\frac{S^2}{34.1^2} + 1.05 \frac{S}{34.1} + 1 \right) \left(\frac{S^2}{64.3^2} + 0.716 \frac{S}{64.3} + 1 \right)} \tag{D-6}$$

The zero at $S = -\frac{K}{\beta}$ results from the actuator friction eventually appearing as a viscous load. This term is generally negligible but is included since it entails no additional computational difficulty. The resonant roots are cancelled because the numerator of X_c/X_i contains a quadratic factor identical to the quadratic factor in the denominator of $\ddot{\phi}/\delta_A$.

For values of $K_3 = 1.3 \times 10^{-6}$, $\tau_3 = 0.02$, and $K_1 = 50$,

$$\frac{\ddot{\phi}}{\delta_{A_C}} = K_S \frac{I_{XV}}{I_X} \frac{S^2\left(\frac{S}{4450}+1\right)}{\left(\frac{S^2}{34.1^2}+1.05\frac{S}{34.1}+1\right)\left(\frac{S^2}{64.3^2}+0.716\frac{S}{64.3}+1\right)} \tag{D-7}$$

The SAS control loop block diagram can then be shown as:

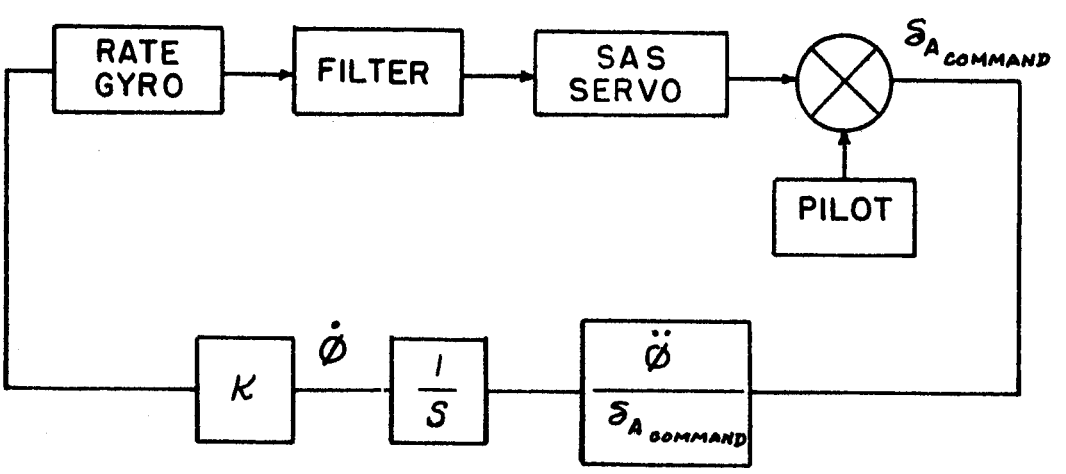

The open loop transfer function KG becomes

$$KG = KK_S \frac{I_{XV}}{I_X} \left[\frac{S^2\left(\frac{S}{4450}+1\right)}{\left(\frac{S^2}{34.1^2}+1.05\frac{S}{34.1}+1\right)\left(\frac{S^2}{64.3^2}+0.716\frac{S}{64.3}+1\right)}\right] \cdot \left[\frac{1}{\frac{S^2}{188.2^2}+0.92\frac{S}{188.2}+1}\right]$$

$$\cdot \left[\frac{1}{\frac{S^2}{426.5^2}+0.8\frac{S}{426.5}+1}\right] \cdot \left[\frac{1}{\frac{S^2}{322^2}+1.8\frac{S}{322}+1}\right] \tag{D-8}$$

The roots of the characteristic equation $(1+KG)$ determine the stability of the SAS loop.

Fig. D-1 is a root locus of equation (8) for values of $KK_S \frac{I_{XV}}{I_X}$

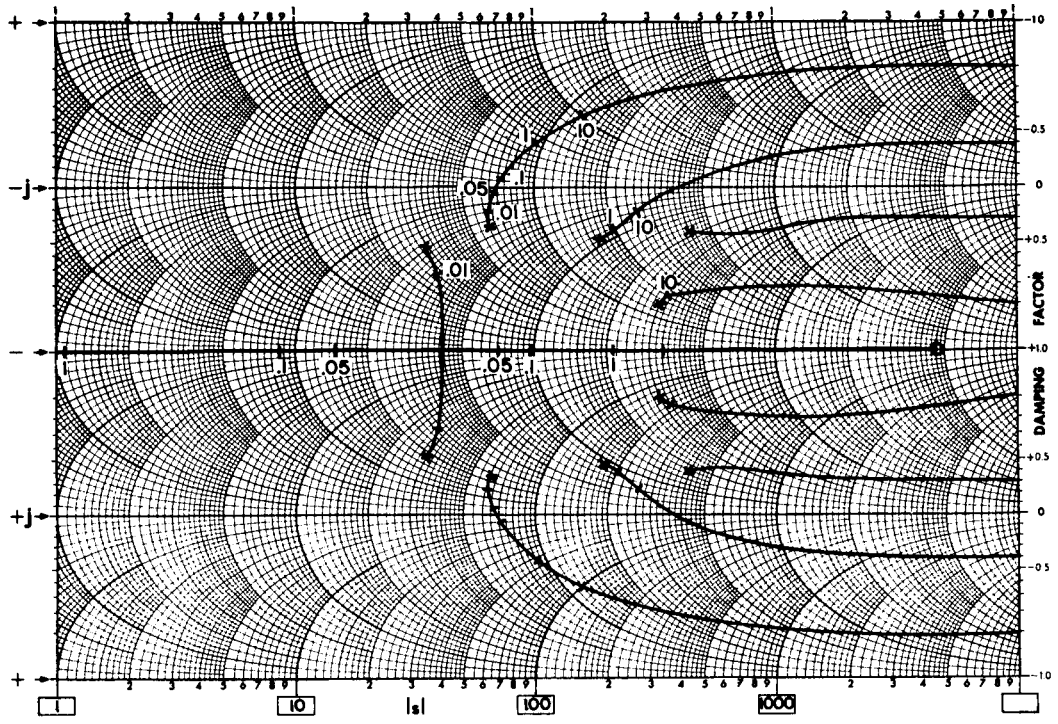

Figure D-1 Root Locus of SAS System Employing a Pressure Feedback Stabilized Actuator

The gain at which roots cross the imaginary axis is approximately 0.07. Dividing this by

$$K_s \frac{I_{xy}}{I_x} = 0.0253$$

yields

$$K = 2.765$$

Since the present system has been calculated to go unstable at a $K = 0.1$ with a load damping of 0.005, the gain improvement possible with a pressure feedback compensated actuator is very significant.

APPENDIX E

PROPOSED ALL MECHANICAL PRESSURE FEEDBACK VALVE CONFIGURATION

The requirements which must be fulfilled to realize a practical pressure feedback valve for the present application are stated below:

1. The device should be all mechanical in operation.
2. The friction inherent in the hydraulic seals of the input rod should have no detrimental effect on the operation of the pressure feedback system.
3. The device should be relatively free from possible sticking (at least as much so as a standard electro-hydraulic valve).
4. Hydraulic wash-out networks would be preferred.
5. Amplification stages, unrealistic gearing and incompatible spring sizes must be avoided if possible.
6. Easy disassembly for cleaning and inspection and no critical adjustments would be desirable.

Requirement 1 is obvious and fulfilled.

Requirement 2 establishes the restriction that all pressure feedback portions of the valve must be interior to the valve (i.e., require no seals to the outside).

Requirement 3 is satisfied by the simple concentric design and the relatively strong springs which are used. Also the shuttle and spool can have circumferential grooves which help prevent sticking

Requirement 4 is inherent in the configuration presented by proper orifice size, spring constants and areas.

Requirement 5 is fulfilled because of the available area and direct connection to the main pressure ports.

Requirement 6 is fulfilled because the complexity is hardly more than the present valve.

Fig. E-1 is a cut-away schematic of the proposed valve configuration.

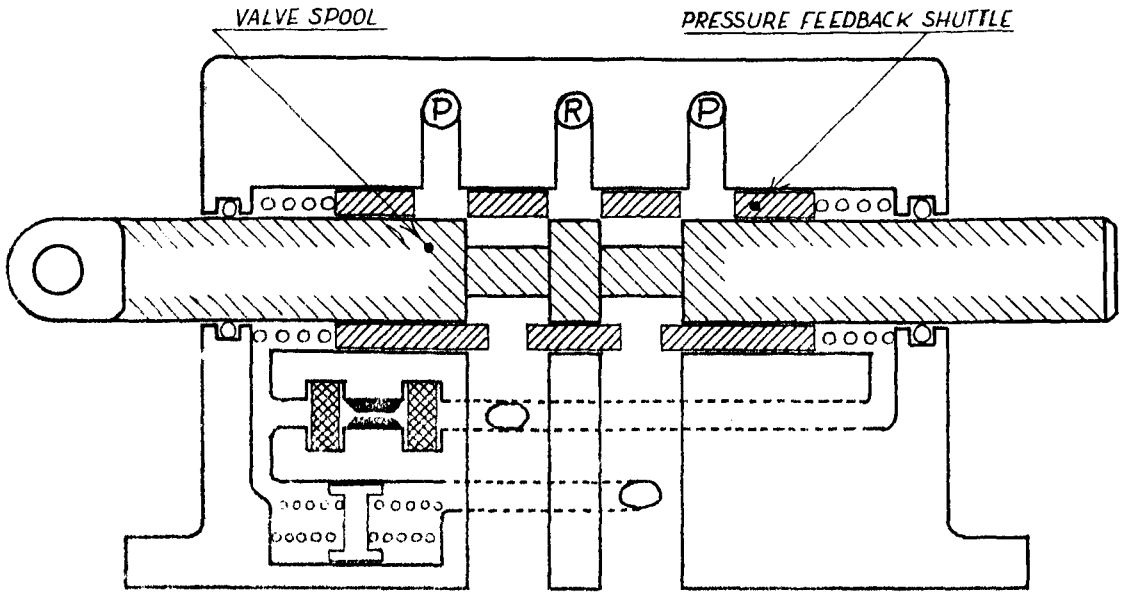

Figure E-1 Proposed Pressure Feedback Valve Configuration

The valve consists of a relatively standard body with two major concentric movable elements called a shuttle and spool. The shuttle is deflected by the "washed-out" pressure feedback signal which is obtained from the small free piston and the orifice. This deflection is independent of the position of the spool, the normal valve input element.

The springs at the end of the shuttle, in combination with the shuttle end area and the free piston and its springs, determine the deflection sensitivity of the shuttle for pressure differentials.

The displaced volume due to shuttle motion in combination with the spring constants and the flow constricting orifice determine the "wash-out" time constant for the valve. Changes in time constant can therefore be made independently of pressure feedback gain, i.e., by changing the orifice.

Other concentric configurations might possibly reduce leakage effects by juggling the location of the high and low pressure regions. These nuances of valve design are left to the experienced design engineer.

APPENDIX F

THE SYNTHESIS OF TRANSPORT LAGS AND OTHER NETWORKS USING FEEDFORWARD AND FEEDBACK TECHNIQUES

Consider a transfer function having the form $G(s) = \frac{N(s)}{D(s)}$. By a simple summation or feedforward, one can form a new transfer function

$$H(s) = 1 + KG(s) = \frac{D(s) + KN(s)}{D(s)}$$

Thus a transfer function having a higher order complexity can be formed by a simple summation.

If, for instance, $KG(s) = \frac{-Ks}{s^2 + as + b}$, then simple feedforward would result in a transfer function

$$H(s) = \frac{s^2 + (a-K)s + b}{s^2 + as + b}$$

If $K = 2a$, the transfer function would have the form of an all pass phase shifter. A more complex problem which can be considered is of the form $(1 + G_1(s))(1 + G_2(s))$. This can be synthesized schematically by

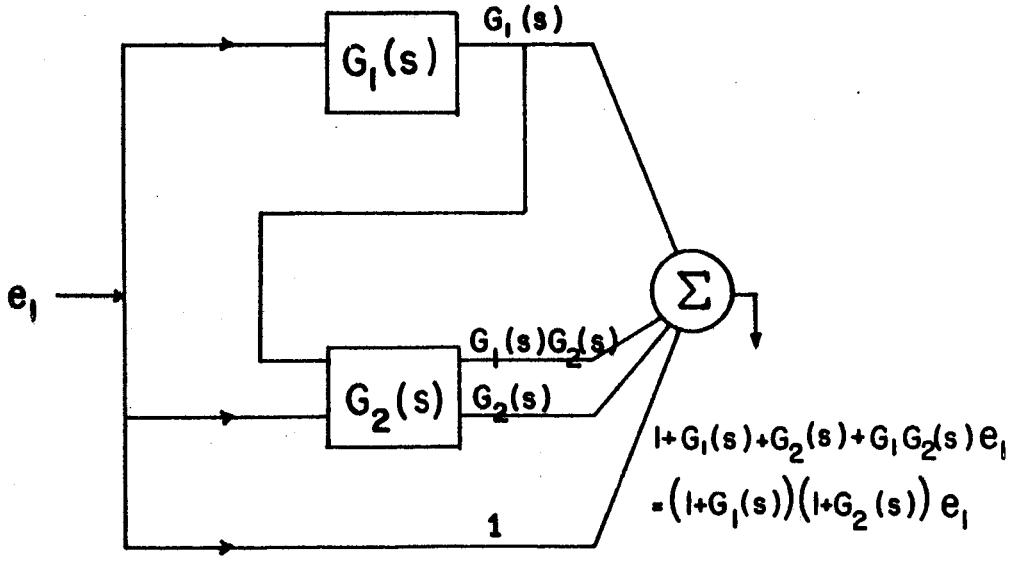

As an example of the above general form, let the $G(s)$ transfer function be formed by the following circuit.

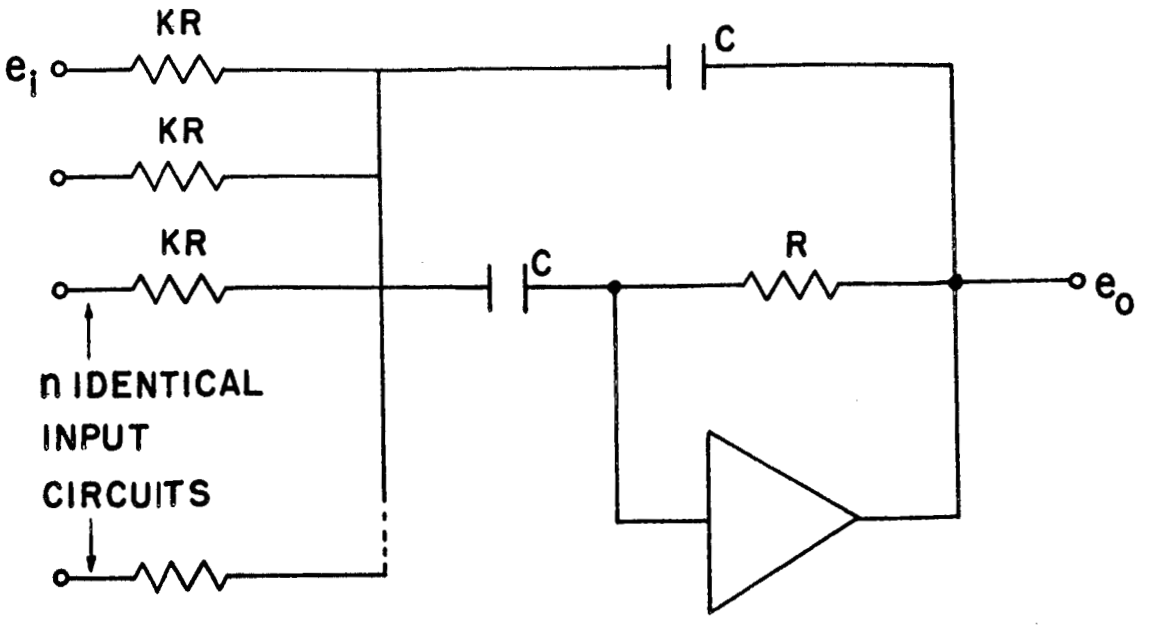

The transfer function for any voltage source (zero impedance) has the form

$$\frac{e_o}{e_i} = -\frac{\frac{1}{KRC}\,S}{S^2 + \frac{2}{RC}\,S + \frac{1}{R^2C^2}\left(\frac{n}{K}\right)}$$

If one then forms the product $\left[1 + G_1(s)\right]\left[1 + G_2(s)\right] = G(s)$

where $$G_1(s) = -\frac{\frac{4}{R_1C}\,S}{S^2 + \frac{2}{R_1C}\,S + \frac{1}{R_1^2C^2}\sqrt{\frac{1}{K_1}}}$$

and $$G_2(s) = -\frac{\frac{4}{R_2C}\,S}{S^2 + \frac{2}{R_2C}\,S + \frac{1}{R_2^2C^2}\sqrt{\frac{2}{K_2}}}$$

the result will be

$$G(s) = \frac{\left(S^2 - \frac{2}{R_1C}\,S + \frac{1}{R_1^2C^2}\sqrt{\frac{1}{K_1}}\right)\left(S^2 - \frac{2}{R_2C}\,S + \frac{1}{R_2^2C^2}\sqrt{\frac{2}{K_2}}\right)}{\left(S^2 + \frac{2}{R_1C}\,S + \frac{1}{R_1^2C^2}\sqrt{\frac{1}{K_1}}\right)\left(S^2 + \frac{2}{R_2C}\,S + \frac{1}{R_2^2C^2}\sqrt{\frac{2}{K_2}}\right)}$$

This ratio of quartics is a transfer function having pole and zero locations which are symmetrical around the imaginary axis as well as the real axis. This can, by proper selection of the roots, be made the fourth order Pade approximation to a time delay or transport lag.

A schematic diagram of the network resulting from this approach to the problem is

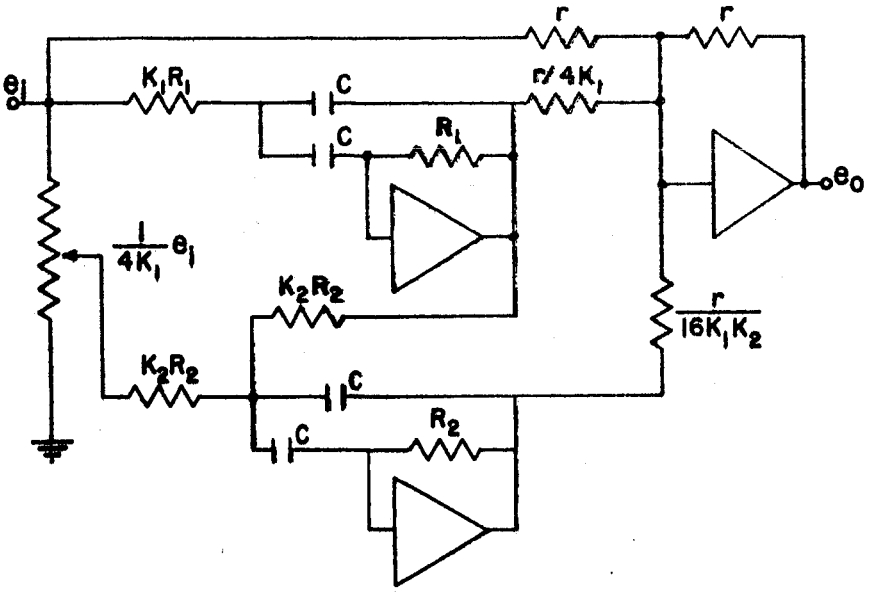

$$\mathcal{R} \ll K_2 R_2 \qquad \frac{e_o}{e_i} = \left(\frac{s^2 - 2\zeta_1\omega_1 s + \omega_1^2}{s^2 + 2\zeta_1\omega_1 s + \omega_1^2}\right)\left(\frac{s^2 - 2\zeta_2\omega_2 s + \omega_2^2}{s^2 + 2\zeta_2\omega_2 s + \omega_2^2}\right)$$

where $K_1 = \zeta_1^2$; $R_1C = \frac{1}{\omega_1\zeta_1}$ and $K_2 = \zeta_2^2$; $R_2C = \frac{1}{\omega_2\zeta_2}$

Numerical Example:

The polynomial expression of a fourth order Pade approximation for a one-second delay is (Reference 7):

$$G(s) = \frac{s^4 - 20s^3 + 180s^2 - 840s + 1680}{s^4 + 20s^3 + 180s^2 + 840s + 1680}$$

The quadratic factors of the numerator and denominator are

$$G(s) = \frac{(s^2 - 11.58s + 46)(s^2 - 8.42s + 36.5)}{(s^2 + 11.58s + 46)(s^2 + 8.42s + 36.5)}$$

therefore:

$\zeta_1 = .855$	$\zeta_2 = .698$
$\omega_1 = \sqrt{46} = 6.78$ rad/sec	$\omega_2 = \sqrt{36.5} = 6.04$ rad/sec
$K_1 = .731$	$K_2 = .486$
$R_1C = 1/(6.78 \times .855) = .173$	$R_2C = 1/(.698 \times 6.04) = .237$
$C = 1\mu f$ $R_1 = 173\ K\Omega$	$R_2 = 237\ K\Omega$
$K_1R_1 = 126.5\ K\Omega$	$K_2R_2 = 115.2\ K\Omega$

A practical computer circuit is therefore:

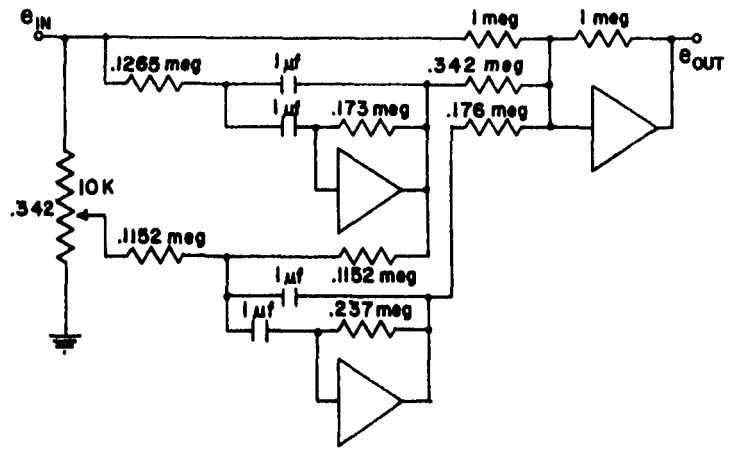

The shifting of the poles of a function is quite often made possible by feedback techniques. In a similar manner, the shifting of the zeros of a function is implemented by feedforward techniques. A combination of these two methods, starting from a fairly simple initial transfer function, is a powerful means toward the realization of complex transfer functions which would otherwise be too complicated to synthesize economically.

APPENDIX G

AEROELASTIC EFFECTS OF HORIZONTAL STABILIZER ON AIRCRAFT ROLL AND AIRCRAFT PITCH TRANSFER FUNCTIONS FOR STABILIZER PITCH INPUT

Introduction

This appendix presents briefly the equations of motion used in deriving transfer functions for airplane rigid body roll and airplane rigid body pitch, including the effects of the two lowest frequency stabilizer normal vibration modes for stabilizer pitch input. Also included are numerical results for these two transfer functions, as well as those for stabilizer spindle vertical shear, spindle torque, and spindle bending moment at the fuselage, in terms of horizontal stabilizer pitch as an input, in vacuo. In addition, the airplane pitch and roll transfer functions, including the two stabilizer modes and damping at high supersonic Mach numbers are presented. Aerodynamic damping terms were derived using piston theory aerodynamics, assuming that the horizontal stabilizer is a flat plate, and neglecting the wing.

Equations of Motion in Vacuo

The linearized equations of motion for displacement inputs to the horizontal stabilizer for airplane rigid body roll in vacuo, including the two lowest stabilizer normal modes, can be written:

$$M_{11}\ddot{\phi} + M_{12}\ddot{H}_1 + M_{13}\ddot{H}_2 = -M_{14}(\ddot{\varepsilon}_h)$$

$$M_{21}\ddot{\phi} + M_{22}\ddot{H}_1 + \omega_1^2 M_{23} H_1 = -M_{24}(\ddot{\varepsilon}_h) \qquad \text{(G-1)}$$

$$M_{31}\ddot{\phi} + M_{33}\ddot{H}_2 + \omega_2^2 M_{33} H_2 = -M_{34}(\ddot{\varepsilon}_h)$$

or, in operational form:

$$\begin{bmatrix} S^2 M_{11} & S^2 M_{12} & S^2 M_{13} \\ S^2 M_{21} & (S^2+\omega_1^2) M_{22} & 0 \\ S^2 M_{31} & 0 & (S^2+\omega_2^2) M_{33} \end{bmatrix} \begin{bmatrix} \phi(S) \\ H_1(S) \\ H_2(S) \end{bmatrix}$$

$$= -S^2 \begin{bmatrix} M_{14} \\ M_{24} \\ M_{34} \end{bmatrix} \delta_h(S) \qquad \text{(G-2)}$$

where

$\phi(t)$ = airplane rigid body roll displacement, positive for right stabilizer down, radians

$\delta_h(t)$ = horizontal stabilizer pitch displacement, positive for right stabilizer leading edge up, radians

$H_1(t)$ = generalized coordinate for the first normal mode of the horizontal stabilizer

$H_2(t)$ = generalized coordinate for the second normal mode of the horizontal stabilizer

ω_1 = frequency of first stabilizer normal mode, rad/sec

ω_2 = frequency of second stabilizer normal mode, rad/sec

t = time, seconds

$\ddot{(\,)} = \frac{d^2(\,)}{dt}$

A similar set of equations can be written for rigid body pitch, $\theta(t)$, which includes the two stabilizer normal modes.

For rigid body roll, the M_{jj} terms are defined as follows:

$$M_{11} = I_{xx}$$

$$M_{12} = 2\left(\int_S h_1\, y\, dm + \int_S \alpha_1\, y\, \eta\, dm\right) + \Delta M_{12}$$

$$M_{13} = 2\left(\int_S h_2\, y\, dm + \int_S \alpha_2\, y\, \eta\, dm\right) + \Delta M_{13}$$

$$M_{14} = 2\int_S xy\, dm = I_{xy}^{z}$$

$$M_{21} = M_{12}$$

$$M_{22} = 2\left(\int_S (h_1)^2\, dm + 2\int_S h_1 \alpha_1\, \eta\, dm + \int (\alpha_1)^2\, \eta^2\, dm\right) + \Delta M_{22}$$

$$M_{24} = 2\left(\int_S h_1\, x\, dm + \int_S \alpha_1\, x\, \eta\, dm\right) + \Delta M_{24}$$

$$M_{31} = M_{13}$$

$$M_{33} = 2\left(\int_S (h_2)^2\, dm + 2\int_S h_2\, \alpha_2\, \eta\, dm + \int_S (\alpha_1)^2\, \eta^2\, dm\right) + \Delta M_{33}$$

$$M_{34} = 2\left(\int_S h_2\, x\, dm + \int_S \alpha_2\, x\, \eta\, dm\right) + \Delta M_{34}$$

where one can define:

(x, y) and (ξ, η) ~ coordinates as defined in Figure G-1

dm ~ an element of mass of the horizontal stabilizer

$h_1(\xi)$, $\alpha_1(\xi)$ ~ bending and torsion modal displacements at and about the stabilizer elastic axis in the normal mode of the stabilizer

$\int_S$ ~ indicates integration over one surface.

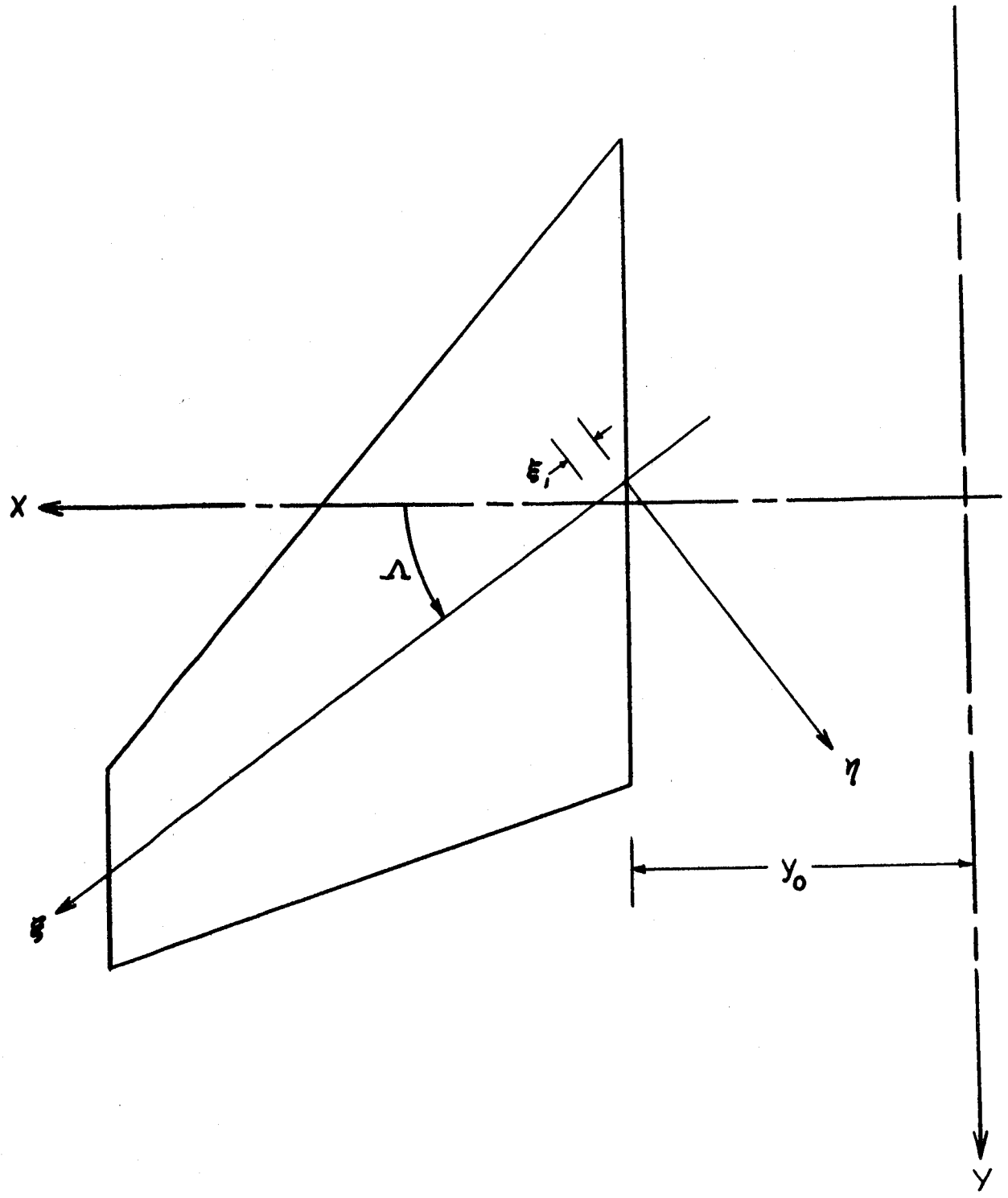

Figure G-1 X-15 Horizontal Stabilizer Plan View – Coordinate Systems Used in Analysis of Appendix G

In Table I are listed the lumped mass breakdown for the X-15 227 lb horizontal stabilizer in terms of weights on, and weight unbalances and weight-moments of inertia about, the swept elastic axis of the stabilizer. Also shown in Table I are additional lumped weight on, and weight unbalance and moment of inertia at the root station about the stabilizer spindle pitch axis. These latter account for the large triangular section of the stabilizer forward of the pitch axis at the root.

Table I NAA Stabilizer Lumped Weight Breakdown

Station, ξ (along elastic axis), ft	W (Weight) lb	S_α (Weight Unbalance) lb-ft	I_α Weight Moment of Inertia lb-ft^2
0.333	31.1	-9.62	33.6
1.50	41.0	2.36	60.0
2.62	34.7	3.80	46.9
3.79	29.0	2.28	29.3
4.91	22.4	1.07	14.7
6.09	18.4	2.96	7.18

At Station 0.333, at and about stabilizer spindle pitch axis:

W^*	S_α^*	I_α^*
lb	lb-ft	lb-ft^2
51.0	-86.7	215

The ΔM_{ij} terms which account for this element of the stabilizer are as follows:

$$\Delta M_{12} = 2y_o (S_\alpha^*)_1 \left[\sin\Lambda \left(\frac{\partial k_1}{\partial \xi}\right)_1 + \cos\Lambda\, (\alpha_1)_1 \right]$$

$$\Delta M_{13} = 2y_o (S_\alpha^*)_1 \left[\sin\Lambda \left(\frac{\partial h_2}{\partial \xi}\right) + \cos\Lambda\, (\alpha_2)_1 \right]$$

$$\Delta M_{22} = 2(I_\alpha^*)_1 \left[\left(\frac{\partial k_1}{\partial \xi}\right)_1^2 \sin^2\Lambda + \left(\frac{\partial k_1}{\partial \xi}\right)_1 (\alpha_1)_1 \sin 2\Lambda + (\alpha_1)_1^2 \cos^2\Lambda \right]$$

$$\Delta M_{24} = 2(I_\alpha^*)_1 \left[\sin\Lambda \left(\frac{\partial h_1}{\partial \xi}\right)_1 + \cos\Lambda (\alpha_1)_1 \right]$$

$$\Delta M_{33} = 2(I_\alpha^*)_1 \left[\left(\frac{\partial h_2}{\partial \xi}\right)_1^2 \sin^2\Lambda + \left(\frac{\partial h_2}{\partial \xi}\right)(\alpha_2)_1 \sin 2\Lambda + (\alpha_2)_1^2 \cos^2\Lambda \right]$$

$$\Delta M_{34} = 2(I_\alpha^*)_1 \left[\sin\Lambda \left(\frac{\partial h_2}{\partial \xi}\right)_1 + \cos\Lambda (\alpha_2)_1 \right]$$

where Λ is the sweep angle for the stabilizer elastic axis

$(S_\alpha^*)_1$, $(I_\alpha^*)_1$ are the lumped weight unbalance and moment of inertia at the stabilizer root station about the stabilizer spindle axis

$\left(\frac{\partial h_i}{\partial \xi}\right)_1$, $(\alpha_i)_1$ are bending slope and torsional displacement in the i^{th} stabilizer normal mode at the stabilizer root station about the stabilizer elastic axis

Table II lists the $h_i(\xi)$ and $\alpha_i(\xi)$ for the two stabilizer normal modes in deriving the numerical results presented in this appendix.

Table II NAA Calculated Stabilizer Modal Deflections

Station, ξ (along elastic axis), ft	First Mode		Second Mode	
	h_1 ft	α_1 rad	h_2 ft	α_2 rad
0.333	0.087	0.0092	1.337	-4.08
1.50	0.219	0.0105	1.155	-4.88
2.62	0.380	0.0120	1.061	-5.64
3.79	0.565	0.0139	1.024	-6.33
4.91	0.774	0.0163	1.015	-6.91
6.09	1.000	0.0201	1.000	-7.30

$\left(\frac{\partial h_1}{\partial \xi}\right)_1 = 0.0993$ $\left(\frac{\partial h_2}{\partial \xi}\right)_1 = -0.220$

$\omega_1 = 91.0$ rad/sec $\omega_2 = 233.5$ rad/sec

The data presented in Tables I and II were obtained from North American Aviation, Inc., Los Angeles, California. Table II data are from NAA calculations for the 227 lb stabilizer based on measured stabilizer root flexibility influence coefficients, and the stabilizer mass breakdown of Table I.

For rigid body pitch, $\phi(s)$, in Equation (G-2) is replaced by $\theta(s)$, and the M_{1j} and M_{j1} terms become:

$$M_{11} = I_{yy}$$

$$M_{12} = 2\int_s (\ell_t + x)(h_1 + \eta\alpha_1)\,dm + \Delta M_{12} = M_{21}$$

$$M_{13} = 2\int_s (\ell_t + x)(h_2 + \eta\alpha_2)\,dm + \Delta M_{13} = M_{31}$$

$$M_{14} = 2\int_s (\ell_t + x)\,x\,dm$$

where $\phi(t)$ = aircraft rigid body pitch displacement, positive nose up, radians

$\ell(t)$ = distance between aircraft pitch axis and stabilizer pitch axis, assumed to be 16.0 feet for this analysis

$$\Delta M_{12} = 2\ell_t (S^*_\alpha)_1 \left[\sin\Lambda\left(\frac{\partial h_1}{\partial \xi}\right)_1 + \cos\Lambda\,(\alpha_1)_1\right]$$

$$\Delta M_{13} = 2\ell_t (S^*_\alpha)_1 \left[\sin\Lambda\left(\frac{\partial h_2}{\partial \xi}\right) + \cos\Lambda\,(\alpha_2)_1\right]$$

The M_{22}, M_{33}, M_{24} and M_{34} terms are the same as for the roll equations, Equation (G-2).

Equations of Motion Including Aerodynamics

For Mach numbers above approximately M $\approx$ 2.5, piston theory aerodynamics should be relatively accurate when applied to the X-15 horizontal stabilizer. As piston theory is a quasi-steady aerodynamic theory, the equations of motion including piston theory aerodynamics can be written explicitly for very general time-dependent displacements.

In operational form, for aircraft roll and two stabilizer normal modes, and for a time-dependent stabilizer pitch displacement input, the equations of motion are:

$$\begin{bmatrix} S^2M_{11} + SA'_{11}\bar{q} & S^2M_{12} + SA'_{12}\bar{q} + A_{12}\bar{q}U & S^2M_{13} + SA'_{13}q + A_{13}\bar{q}U \\ S^2M_{21} + SA'_{21}\bar{q} & (S^2+\omega_1^2)M_{22} + SA'_{22}q + A_{22}\bar{q}U & SA'_{23}\bar{q} + A \\ S^2M_{31} + SA'_{31}\bar{q} & SA'_{32}\bar{q} + A_{32}\bar{q}U & (S^2+\omega_2^2)M_{33} + SA'_{33}\bar{q} + A_{33}\bar{q}U \end{bmatrix} \begin{bmatrix} \phi(S) \\ H_1(S) \\ H_2(S) \end{bmatrix}$$

$$= - \begin{bmatrix} S^2M_{14} + SA'_{14}\bar{q} + A_{14}\bar{q}U \\ S^2M_{24} + SA'_{24}\bar{q} + A_{24}\bar{q}U \\ S^2M_{34} + SA'_{34}\bar{q} + A_{34}\bar{q}U \end{bmatrix} \qquad \text{(G-3)}$$

where the M_{ij} terms are defined in a previous section, the A'_{ij} terms are aerodynamic damping coefficients, and the A_{ij} terms are aerodynamic stiffness coefficients, and where:

$\bar{q} = {}^{8q}/_{MU}$

q = free stream dynamic pressure, lb/ft^2

M = Mach number

U = free stream velocity, ft/sec

It is theoretically possible to include effects of airfoil profile and thickness in aerodynamic coefficients derived from piston theory. However, because of somewhat limited time available for these calculations, simpler coefficients were computed assuming the stabilizer was a flat plate. For the same reason, only the aerodynamic damping terms were actually computed and included in the numerical results presented. It is believed that the more important aerodynamic effects on control system behavior are still retained, although the inclusion of profile and thickness in the aerodynamic coefficients can result in a reduction of aerodynamic damping. It should be noted that the wing aerodynamics are not included in the present results. The neglect of wing aerodynamics means that the A'_{11} term is much smaller than it would otherwise be, that is, the aerodynamic damping in roll is considerably underestimated.

The A'_{ij} terms are as follows (for aircraft roll and two stabilizer normal modes):

$$A'_{11} = \int_S y^2 dA$$

$$A'_{12} = \int_S y(h_1 + \eta\alpha_1) dA$$

$$A'_{13} = \int_S y(h_2 + \eta\alpha_2) dA$$

$$A'_{14} = \int_S xy\, dA$$

$$A'_{21} = A'_{12}$$

$$A'_{22} = \int_S (h_1 + \eta\alpha_1)^2 dA$$

$$A'_{23} = \int_S (h_2 + \eta\alpha_2)(h_1 + \eta\alpha_1) dA$$

$$A'_{24} = \int_S x(h_1 + \eta\alpha_1) dA$$

$$A'_{31} = A'_{13}$$

$$A'_{32} = A'_{23}$$

$$A'_{33} = \int_S (h_2 + \eta\alpha_2)^2 dA$$

$$A'_{34} = \int_S x(h_2 + \eta\alpha_2) dA$$

where dA is an element of area of the stabilizer surface.

The equations of motion for aircraft pitch, two stabilizer modes and stabilizer pitch input displacement, including aerodynamics, are as in Equation (G-3) with $\phi(s)$ replaced by $\theta(s)$. The M_{ij} terms are as defined for the in vacuo pitch case equations of motion, and the A_{ij} terms as follows:

$$A'_{11} = \int_S (\ell_t + x)^2 dA$$

$$A'_{12} = \int_S (\ell_t + x)(h_1 + \eta\alpha_1) dA$$

$$A'_{13} = \int_S (\ell_t + x)(h_2 + \eta\alpha_2) dA$$

$$A'_{14} = \int_S (\ell_t + x)\, x\, dA$$

$$A'_{21} = A'_{12}$$

$$A'_{31} = A'_{13}$$

The remaining A'_{ij} terms are as defined for the roll case.

Equations for Stabilizer Spindle Vertical Shear, Torque, and Bending Moment at the Fuselage

For aircraft rigid body roll, two stabilizer normal modes and stabilizer pitch input displacement in vacuo, the equations for stabilizer spindle vertical shear, torque and bending moment at the fuselage (from one stabilizer) are:

$$\begin{bmatrix} V(t) \\ T(t) \\ M(t) \end{bmatrix} = \begin{bmatrix} V_1 & V_2 & V_3 & V_4 \\ T_1 & T_2 & T_3 & T_4 \\ M_1 & M_2 & M_3 & M_4 \end{bmatrix} \begin{bmatrix} \ddot{\phi}(t) \\ \ddot{H}_1(t) \\ \ddot{H}_2(t) \\ \ddot{\delta}_h(t) \end{bmatrix}$$

or, in operational form:

$$\begin{bmatrix} V(s) \\ T(s) \\ M(s) \end{bmatrix} = s^2 \begin{bmatrix} V_1 & V_2 & V_3 & V_4 \\ T_1 & T_2 & T_3 & T_4 \\ M_1 & M_2 & M_3 & M_4 \end{bmatrix} \begin{bmatrix} \phi(s) \\ H_1(s) \\ H_2(s) \\ \delta_h(s) \end{bmatrix} \qquad \text{(G-4)}$$

where: $V(t)$ = vertical shear, positive up, lb

$T(t)$ = spindle torque, positive in opposite sense for positive δ_h, ft-lb

$M(t)$ = spindle bending moment, positive for upper fibers of stabilizer spindle in compression, ft-lb

$$V_1 = \int_s y\,dm$$

$$V_2 = \int_s (h_1 + \eta\alpha_1)\,dm + \Delta V_2$$

$$V_3 = \int_s (h_2 + \eta\alpha_2)\,dm + \Delta V_3$$

$$V_4 = \int_s x\,dm$$

$$T_1 = \int_s xy\,dm$$

$$T_2 = \int_s x(h_1 + \eta\alpha_1)\,dm + \Delta T_2$$

$$T_3 = \int_s x(h_2 + \eta\alpha_2)\,dm + \Delta T_3$$

$$T_4 = \int_s x^2\,dm$$

$$M_1 = \int_S y\, y^* dm$$

$$M_2 = \int_S y^* (h_1 + \eta \alpha_1)\, dm + \Delta M_2$$

$$M_3 = \int_S y^* (h_2 + \eta \alpha_2)\, dm + \Delta M_3$$

$$M_4 = \int_S x\, y^* dm$$

$$y^* = y - y_0$$

y_0 = distance from aircraft roll axis to stabilizer root chord

$$\Delta V_2 = (S_\alpha^*)_1 \left[\left(\frac{\partial h_1}{\partial \xi} \right)_1 \sin \Lambda + (\alpha_1)_1 \cos \Lambda \right]$$

$$\Delta V_3 = (S_\alpha^*)_1 \left[\left(\frac{\partial h_2}{\partial \xi} \right)_1 \sin \Lambda + (\alpha_2)_1 \cos \Lambda \right]$$

$$\Delta T_2 = (I_\alpha^*)_1 \left[\left(\frac{\partial h_1}{\partial \xi} \right)_1 \sin \Lambda + (\alpha_1)_1 \cos \Lambda \right]$$

$$\Delta T_3 = (I_\alpha^*)_1 \left[\left(\frac{\partial h_2}{\partial \xi} \right)_1 \sin \Lambda + (\alpha_2)_1 \cos \Lambda \right]$$

$$\Delta M_2 = \xi_1 \cos \Lambda\, (S_\alpha^*)_1 \left[\left(\frac{\partial h_1}{\partial \xi} \right)_1 \sin \Lambda + (\alpha_1)_1 \cos \Lambda \right]$$

$$\Delta M_3 = \xi_1 \cos \Lambda\, (S_\alpha^*)_1 \left[\left(\frac{\partial h_2}{\partial \xi} \right)_1 \sin \Lambda + (\alpha_2)_1 \cos \Lambda \right]$$

ξ_1 = distance from stabilizer root chord to the stabilizer root mass station for $(S_\alpha^*)_1$, $(I_\alpha^*)_1$ (See Figure G-1).

For aircraft rigid body pitch, two stabilizer normal modes and stabilizer pitch input displacement, the equations are similar to (G-4) with $\Phi(s)$ replaced by $\Theta(s)$, and where

$$V_1 = \int_S (\ell_t + x)\, dm$$

$$T_1 = \int_S y(\ell_t + x)\, dm$$

$$M_1 = \int_S y^* (\ell_t + x)\, dm$$

with the remaining V, T and M coefficients defined as for the roll case.

Transfer Functions

The desired transfer functions follow directly from the solutions of Equations (G-2) and (G-3), and from Equation (G-4). Let

$$\Phi(s) = \frac{\phi(s)}{\delta_h(s)}, \quad \Theta(s) = \frac{\theta(s)}{\delta_h(s)}$$

$$v(s) = \frac{V(s)}{\delta_h(s)}, \quad t(s) = \frac{T(s)}{\delta_h(s)}, \quad m(s) = \frac{M(s)}{\delta_h(s)}$$

After calculation of numerical values of the various terms involved, and solving Equations (G-2) and (G-3) for $\Phi(s)$, and the corresponding pitch equations for $\Theta(s)$, there results

In vacuo, for aircraft roll:

$$\Phi(s) = -\frac{0.0205}{g(s)}\left[(s^2+\omega_1^2)(s^2+\omega_2^2) + 0.3698\, s^2(s^2+\omega_1^2) - 1.350\, s^2(s^2+\omega_2^2)\right]$$

$$v_\phi(s) = -\frac{s^2}{g(s)}\left[0.9070(s^2+\omega_1^2)(s^2+\omega_2^2) - 2.263 s^2(s^2+\omega_1^2) + 5.217 s^2(s^2+\omega_2^2) + 0.3434 s^4\right] + 6.174 s^2 \qquad \text{(G-6)}$$

$$t_\phi(s) = -\frac{s^2}{g(s)}\left[0.7379(s^2+\omega_1^2)(s^2+\omega_2^2) + 13.01 s^2(s^2+\omega_1^2) + 13.68 s^2(s^2+\omega_2^2) - 1.685 s^4\right] + 32.61 s^2 \qquad \text{(G-7)}$$

$$m_{\phi}(S) = -\frac{S^2}{g(S)}\left[1.215(S^2+\omega_1^2)(S^2+\omega_2^2) - 1.279\,S^2(S^2+\omega_1^2)\right.$$

$$\left. + 17.19\,S^2(S^2+\omega_2^2) + 0.2279\,S^4\right] + 13.68\,S^2 \qquad \text{(G-8)}$$

where $g(S) = (S^2+\omega_1^2)(S^2+\omega_2^2) - 0.01222\,S^2(S^2+\omega_1^2)$
$- 0.09187\,S^2(S^2+\omega_2^2)$

I_{xx} = 3600 slug-ft^2 has been assumed.

In vacuo, for aircraft pitch:

$$\Phi(S) = -\frac{10^9}{\Delta(S)}\left[14.28(S^2+\omega_1^2)(S^2+\omega_2^2) - 1.560\,S^2(S^2+\omega_1^2) - 15.01\,S^2(S^2+\omega_2^2)\right] \qquad \text{(G-9)}$$

$$v_{\theta}(S) = -\frac{10^9 S^2}{\Delta(S)}\left[1.699\times10^3(S^2+\omega_1^2)(S^2+\omega_2^2) + (0.3760\,I_{yy} - 1.795\times10^3)S^2(S^2+\omega_2^2)\right.$$

$$\left. - (0.1370\,I_{yy} + 0.1231\times10^3)S^2(S^2+\omega_1^2) + 0.3738\times10^3 S^4\right] + 32.61\,S^2 \qquad \text{(G-10)}$$

$$t_{\theta}(S) = -\frac{10^9 S^2}{\Delta(S)}\left[10.71\times10^3(S^2+\omega_1^2)(S^2+\omega_2^2) + (0.8563\,I_{yy} - 3.294\times10^3)S^2(S^2+\omega_2^2)\right.$$

$$\left. + (0.6700\,I_{yy} - 1.476\times10^3)S^2(S^2+\omega_1^2) - 1.236\times10^3 S^4\right] + 32.61\,S^2 \qquad \text{(G-11)}$$

$$m_{\theta}(S) = -\frac{10^9 S^2}{\Delta(S)}\left[4.496\times10^3(S^2+\omega_1^2)(S^2+\omega_2^2) + (1.099\,I_{yy} - 7.451\times10^3)S^2(S^2+\omega_2^2)\right.$$

$$\left. - (0.9095\,I_{yy} + 0.07541\times10^3)S^2(S^2+\omega_1^2) + 2.177\times10^3 S^4\right] + 13.68\,S^2 \qquad \text{(G-12)}$$

where

$$\Delta(s) = 10^6 \left[54.35\, I_{YY} (s^2+\omega_1^2)(s^2+\omega_2^2) - 141.7 \times 10^3 s^2 (s^2+\omega_2^2) - 2.713 \times 10^3 s^2 (s^2+\omega_1^2) \right]$$

I_{YY} is in slug-ft^2.

Including stabilizer aerodynamic damping (for M $\geq$ 2.5):

For Roll:

$$\Phi(s) = -\frac{1}{R(s)} \left[118.7 s^2 (s^2+\omega_1^2)(s^2+\omega_2^2) + 439.2 \bar{q} s (s^2+\omega_1^2)(s^2+\omega_2^2) + 43.89 s^4 (s^2+\omega_1^2) - 160.1 s^4 (s^2+\omega_2^2) + 31.76 \bar{q} s^3 (s^2+\omega_1^2) - 300.1 \bar{q} s^3 (s^2+\omega_2^2) + 25.59 (\bar{q})^2 s^2 (s^2+\omega_1^2) + 65.2 (\bar{q})^2 s^2 (s^2+\omega_2^2) + 71.24 \bar{q} s^5 - 30.84 (\bar{q})^2 s^4 - 60.35 (\bar{q})^3 s^3 \right] \quad \text{(G-13)}$$

where

$\bar{q} = {}^{Bq}/_{MU}$

q = free stream dynamic pressure, lb/ft^2

M = free stream Mach number

U = free stream velocity, ft/sec

$$R(s) = 10^3 \left[5.861 s^2 (s^2+\omega_1^2)(s^2+\omega_2^2) + 4.109 \bar{q} s (s^2+\omega_1^2)(s^2+\omega_2^2) - 0.07170 s^4 (s^2+\omega_1^2) - 0.5385 s^4 (s^2+\omega_2^2) + 0.4653 \bar{q} s^3 (s^2+\omega_1^2) - 2.514 \bar{q} s^3 (s^2+\omega_2^2) + 0.3013 (\bar{q})^2 s^2 (s^2+\omega_1^2) + 6.154 (\bar{q})^2 s^2 (s^2+\omega_2^2) - 0.1283 \bar{q} s^5 + 0.8245 (\bar{q})^2 s^4 + 0.3088 (\bar{q})^3 s^3 \right]$$

For Pitch:

$$\Theta(s) = -\frac{10^6}{P(s)}\Big\{(0.4278\,s^2+10.14\,\bar{q}\,s)(s^2+\omega_1^2)(s^2+\omega_2^2)$$
$$-\left[0.04672\,s^4+0.07328\,\bar{q}\,s^3-0.6998\,(\bar{q}\,s)^2\right](s^2+\omega_1^2)$$
$$-\left[0.4495\,s^4+1.132\,\bar{q}\,s^3-20.10\,(\bar{q}\,s)^2\right](s^2+\omega_2^2)$$
$$-0.2020\,\bar{q}\,s^5-0.5299\,(\bar{q})^2 s^4-0.9566\,(\bar{q})^3 s^3\Big\} \qquad \text{(G-14)}$$

where

$$P(s) = 10^6\Big\{(50.55\times10^{-6}I_{yy}\,s^2+29.74\,\bar{q}\,s)(s^2+\omega_1^2)(s^2+\omega_2^2)$$
$$-\left[0.08125\,s^4+(0.2453-3.749\times10^{-6}I_{yy})\,\bar{q}\,s^3-2.021\,(\bar{q}\,s)^2\right](s^2+\omega_1^2)$$
$$-\left[4.243\,s^4+(18.77-112.2\times10^{-6}I_{yy})\,\bar{q}\,s^3-46.29\,(\bar{q}\,s)^2\right](s^2+\omega_2^2)$$
$$-0.6858\,s^5+(6.991\times10^{-6}I_{yy}-2.646)\,(\bar{q})^2 s^4-5.037\,(\bar{q})^3 s^3\Big\}$$

Analysis of the Effects of Aerodynamic Damping

The fuselage roll to spindle axis angle transfer function, including aerodynamic damping (piston theory), has the form of Equation (G-13).

The terms in $\bar{q}$, $(\bar{q})^2$ and $(\bar{q})^3$ in the numerator are less significant than the effect of the terms in $\bar{q}$, $(\bar{q})^2$ and $(\bar{q})^3$ in the denominator at the resonant frequencies.

Collecting terms in the denominator and using the values of $I_x = 32.2 \times 3600$ lb-ft^2.

$$\Delta = 5.88\times10^{6}\,s(s^2+\omega_1^2)(s^2+\omega_2^2)+10^{6}\ -0.0177\,s^3(s^2+\omega_1^2)-0.5388\,s^3(s^2+\omega_2^2)$$
$$+10^{6}\bar{q}\left\{4.109(s^2+\omega_1^2)(s^2+\omega_2^2)+4.66\,s^2(s^2+\omega_1^2)+10.492\,s^2(s^2+\omega_2^2)\right\}$$
$$+10^{6}(\bar{q})^2\left\{0.3013\,s(s^2+\omega_1^2)+6.154\,s(s^2+\omega^2)+0.824\,s^3\right\}$$
$$+10^{6}(\bar{q})^3\left\{0.3088\,s^2\right\}$$

This simplifies to

$$\frac{\Delta}{10^6} = \left\{0.8963\,s^5+4.788\times10^{4}\,s^3+2.93\times10^{8}\,s\right\}$$ exhibits resonant frequency

$$+\bar{q}\left\{19.131\,s^4+72.5\times10^{4}\,s^2+2.93\times10^{8}\right\}$$ main damping term

$$+(\bar{q})^2\left\{7.279\,s^3+28.40\times10^{4}\,s\right\}$$ frequency modification

$$+(\bar{q})^3\left\{0.3088\,s^2\right\}$$ damping modification

For values of $\bar{q} \leq 10$, the frequency and damping changes resulting from $(\bar{q})^2$ and $(\bar{q})^3$ are negligible. Therefore, the roots of the denominator can be found from:

$$\frac{\Delta}{10^6} = 0.8963\,s^5+4.788\times10^{4}\,s^3+2.93\times10^{8}\,s$$
$$+q\left\{19.131\,s^4+72.5\times10^{4}\,s^2+2.93\times10^{8}\right\}=0$$

Restating, one can write

$$1+\frac{0.1706\,\bar{q}\left(\frac{s^2}{21.88^2}+1\right)\left(\frac{s^2}{193.6^2}+1\right)}{s\left(\frac{s^2}{215.4^2}+1\right)\left(\frac{s^2}{83.94^2}+1\right)}=0$$

This is in the form of a root locus problem in $\bar{q}$. The effective "gain" $0.1706\,\bar{q}$ for the region about the +j83.94 point can be calculated by geometry

to be $0.151\ r_1 = 0.1706\ \bar{q}$ where r_1 is the radial distance from the j83.94 point. Since the departure angle of this locus is 180°,

$$\zeta_1 = \frac{r_1}{83.9} \quad \therefore \zeta_1 = 0.0135q$$

for $0 \leq \bar{q} \leq 10$ with reasonable accuracy.

In a similar fashion, one can calculate the "gain" in the region around +j215.4 to obtain an expression for the damping available at the second resonant mode.

One obtains $0.1706\ \bar{q} = 0.495\ r_2$

since $\zeta_2 = \frac{r_2}{215.4}$

$$\zeta_2 = 0.0016\,\bar{q}$$

One can see from these results that the aerodynamic damping is relatively important for the first mode resonance but is rather small for the second mode.